Geoscience Frontiers 7 (2016) 431–451

HOSTED BY

Contents lists available at ScienceDirect

China University of Geosciences (Beijing)

Geoscience Frontiers

journal homepage: www.elsevier.com/locate/gsf

Research paper

Regional tectonics, geology, magma chamber processes and mineralisation of the Jinchuan nickel-copper-PGE deposit, Gansu Province, China: A review

T.M. (Mike) Porter

Porter GeoConsultancy Pty Ltd., Linden Park 5065, SA, Australia

ARTICLE INFO

Article history:
Received 14 August 2015
Received in revised form
28 September 2015
Accepted 6 October 2015
Available online 6 November 2015

Keywords:
Rodinia break-up rifting
Plume related
Deep staging chamber
Olivine-orthopyroxene-chromite cumulate
Net textured and disseminated sulphides
Post-magmatic alteration

ABSTRACT

The Jinchuan Ni-Cu-PGE deposit (>500 Mt @ 1.2% Ni, 0.7% Cu, ~0.4 g/t PGE), one of the largest magmatic sulphide deposits in the world, is located within the westernmost terrane of the North China Craton. It is hosted within the 6.5 km long, Neoproterozoic (~0.83 Ga) Jinchuan ultramafic intrusion, emplaced as a sill-like body into a Palaeoproterozoic suite of gneisses, migmatites, marbles and amphibolites, below an active intracratonic rift. The parental magma was high-Mg basalt, generated through melting of sub-crustal lithospheric mantle by a mantle plume during the initiation of Rodinia supercontinent breakup. The lower Palaeozoic collision of the exotic Qilian Block with the breakup-related southern margin of the craton accreted a subduction complex, and emplaced voluminous granitic intrusions and foreland basin sequences within the craton, to as far north as Jinchuan. During the Cainozoic, allochthonous lower Palaeozoic rocks were thrust up to 300 km to the northeast over cratonic basement, to within 25 km of the Jinchuan deposit.

The Jinchuan ultramafic intrusion was injected into three interconnected sub-chambers, each containing a separate orebody. It essentially comprises an olivine-orthopyroxene-chromite cumulate, with interstitial orthopyroxene, clinopyroxene, plagioclase and phlogopite, and is predominantly composed of lherzolite (~80%), with an outer rim of olivine pyroxenite and cores of mineralised dunite. Mineralisation occurs as disseminated and net-textured sulphides, predominantly within the dunite, with lesser, PGE rich lenses, late massive sulphide accumulations, small copper rich pods and limited mineralised diopside skarn in wall rock marbles. The principal ore minerals are pyrrhotite (the dominant sulphide), pentlandite, chalcopyrite, cubanite, mackinawite and pyrite, with a variety of platinum group minerals and minor gold. The deposit underwent significant post-magmatic tremolite-actinolite, chlorite, serpentine and magnetite alteration. The volume of the Jinchuan intrusion accounts for <3% of the total parental magma required to generate the contained olivine and sulphide. It is postulated that mafic melt, intruded into the lower crust, hydraulically supported by density contrast buoyancy from below the Moho, ponded in a large staging chamber, where crystallisation and settling formed a lower sulphide rich mush. This mush was subsequently injected into nearby shallow dipping faults to form the Jinchuan intrusion.

1. Introduction

The Jinchuan ultramafic intrusion hosted nickel-copper-PGE deposit is located close to the city of Jinchang, in north-central Gansu Province, China, at 38°28′18″N, 102°10′59″E, some 300 km NNW of Lanzhou, and 1200 km to the west of Beijing.

The deposit was discovered prior to 1958, when the state owned predecessor of the Jinchuan Group Co., Ltd was founded to undertake its development. Mining commenced in 1960 at the No. 1 mine, including an early open pit, prior to going underground in 1963. The larger No. 2 underground mine commenced production in 1996 (pers. com., Jinchuan Mining staff, 2006).

Chai and Naldrett (1992) recorded that the deposit contained >500 million tonnes (Mt) of ore @ 1.2 wt.% Ni, 0.7 wt.% Cu, based on Chinese ore reserve protocols. In addition, they stated that the ore carried PGE + Au totalling ~1 g/t. These tonnages and grades would

E-mail address: mike.porter@portergeo.com.au.
Peer-review under responsibility of China University of Geosciences (Beijing).

http://dx.doi.org/10.1016/j.gsf.2015.10.005

make it the third largest high-grade sulphide nickel deposit in the world, after Sudbury in Canada and Noril'sk-Talnakh in Russia.

In 2006 the remaining reserve, based on 50 m centre drill intersections, was 432 Mt of ore, after a total historical production of ~90 Mt (pers. com., Jinchuan Mining staff, 2006). The bulk grade of the whole deposit in 2000 was 1.05% Ni, 0.66% Cu, 0.031% Co, 0.23 g/t Pt, 0.11 g/t Pd, 0.01 g/t Os, 0.01 g/t Ir, 0.01 g/t Ru, 0.005 g/t Rh, 0.001% Se, 0.0003% Te, 4.28% S (pers. com., Jinchuan Mining staff, 2000), 0.1 to 0.6 g/t Au (Zhou et al., 2002b).

This contribution has been prepared in response to an invitation from the editors of the volume for a literature review of the tectonic setting, geology and mineralisation at Jinchuan. The literature review is complemented by information from technical visits by the author in 2000 and 2006. It is based on the Jinchuan entry on the Porter GeoConsultancy Pty Ltd ore deposit database available online from www.portergeo.com.au, and is published with the permission of that company.

This paper is presented in two main parts. The first addresses the regional geological and tectonic setting of the deposit, which lies at the confluence of a relatively complex collage of Archaean to Cenozoic tectonic elements. The key characteristics of each of these tectonic elements are described to provide an appreciation of their interrelationships and influence on the deposit, prior to, during and following emplacement. The second part of the paper is focussed on the geology, structure, petrology, mineralogy and mineralisation of the deposit and its geological history.

2. Regional setting

The Jinchuan deposit is hosted by the Neoproterozoic (~0.83 Ga; Li et al., 2005; Yang et al., 2005; Zhang et al., 2010) Jinchuan ultramafic intrusion, emplaced within Palaeoproterozoic high-grade metamorphic rocks, below a Neoproterozoic intracratonic rift (Tang, 1993; Ripley et al., 2005). It is now located <25 km inboard of the current southwestern margin of the North China Craton. The tapering western 'horn' of the craton, where the deposit occurs, is in faulted contact with the Tarim Micro-continent to the northwest. It is bounded to the north by the lower Palaeozoic to early Mesozoic Central Asian Orogenic Belt, and to the south by the early Palaeozoic Qilian Orogen. Collision with each of these orogens resulted in a wide volcano-plutonic belt imposed upon the margins of the craton, with the latter emplacing voluminous granitic plutons in the vicinity of the Jinchuan deposit and possibly the granodiorite dykes cutting the ore zone. Large scale, northeast vergent Cenozoic shortening has thrust the rocks of the Qilian Orogen over the North China Craton, possibly by as much as several hundred kilometres. A broad overview of the key characteristics and geologic history of each of these tectonic elements, and their inter-relationships is detailed below, to illustrate the context of the Jinchuan intrusion.

2.1. North China Craton

This craton, which covers an area of ~1.25 million km^2, has a triangular shape, with a 2500 km east-west base from western Gansu to North Korea in the north, and an apex 1000 km to the south in central eastern China (Fig. 1).

2.1.1. Archaean

The craton encloses a number of ancient cratonic nuclei, dominantly composed of orthogneisses and metamorphosed sedimentary rocks. These rocks carry ~3.8 to 3.0 Ga magmatic and detrital zircons, sourced from primitive tonalite-trondhjemite-granodiorite (TTG), orthogneisses, and mafic rocks derived from oceanic lithosphere protoliths. These older rocks account for an

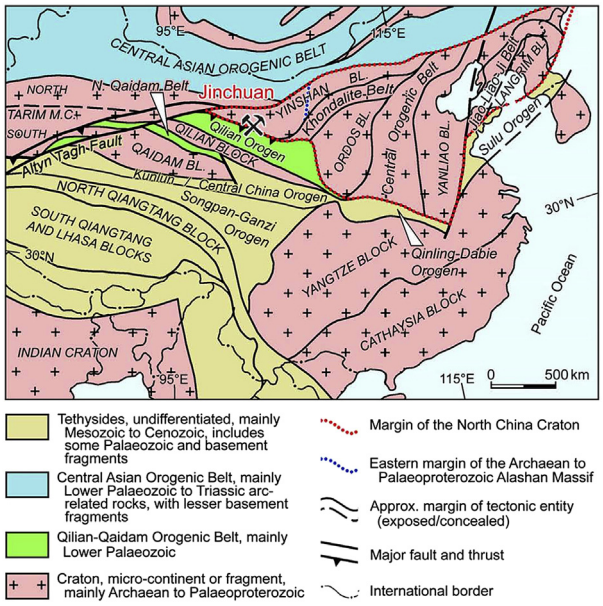

Figure 1. Tectonic setting and location of the Jinchuan Ni-Cu-PGE deposit, Gansu Province, China.

estimated 15% of the volume of the North China Craton (Zhai and Santosh, 2011).

The great majority (~78%) of the rocks that constitute the craton, have Sm-Nd T_{DM} ages between 3.0 and 2.5 Ga, including a dominant population of TTG gneisses with a ~2.7 Ga magmatic zircon U-Pb age, most of which underwent 2.6 to 2.5 Ga metamorphism and deformation. These rocks occur in at least seven ovoid-shaped (each 100 to 400 km across) Archaean "micro-continental blocks", most of which contain ancient pre-3.0 Ga nuclei (Zhai and Santosh, 2011). The individual micro-continental blocks demonstrate some differences in rock associations and crustal evolutionary history. With the exception of the westernmost, the Alashan Block, that hosts Jinchuan, these micro-continental blocks are separated by an anastomosing network of either 2.8 to 2.7 Ga, or 2.5 Ga greenstone belts, the earlier of which predate some of the 2.7 Ga TTG batholiths. The greenstone belts are composed of medium to high grade metamorphosed sequences of bimodal volcanic rocks (pillow basalts and dacites) intercalated with komatiites low in the sequence, and calc-alkalic volcanic rocks (basalt, andesite and felsic rocks) in the upper part of the section, as well as banded quartz-magnetite rocks, conglomerates and greywacke sandstones (Zhai and Santosh, 2011). The basaltic rocks have been grouped into those with geochemical characteristics similar to modern island arc-continental margins, and those of back-arc basin affinities, with very few similar to ocean basin or mid-ocean ridge basalts (Zhai and Santosh, 2011).

Zhai and Santosh (2011) noted that by 2.5 Ga, all rocks in the micro-continental blocks of the North China Craton, without exception, were metamorphosed, and intruded by granitic sills and related bodies in three distinct pulses (2.55 to 2.53, 2.51 to 2.50 and ~2.45 Ga), each comprising varying proportions of high-Na TTG, monzonitic granites, potassic granites and coeval ultramafic-mafic and syenitic dykes (Zhai et al., 2010). Zhai and Santosh (2011) took this to indicate all of the micro-continental blocks were probably welded by greenstone belts by the end of the Neoarchaean, and observed that the available evidence indicates the North China Craton was tectonically inactive between ~2.5 and 2.35 Ga, and mostly behaved as a stable continent block in that period (Zhai et al., 2010).

2.1.2. Palaeoproterozoic

Three curvilinear belts of Palaeoproterozoic volcano-sedimentary and granitic rocks formed within, or on the continental margin of, the North China Craton between ~2.35 and ~1.97 Ga, generally unconformably overlying Archaean basement. These are, from west to east, the Khondalite, Central Orogenic (or Trans-North China) and Jiao-Liao-Ji belts/orogens which separated four new micro-continental blocks, the Yinshan, Ordos, Yanliao (or Longgang) and Langrim blocks (Fig. 1; Zhai and Santosh, 2011; Zhao et al., 2012). The Central Orogenic Belt overlaps the main concentration of Neoarchaean greenstone belts. The sequences in these Palaeoproterozoic belts comprise a lower formation, composed of bi-modal basic and acid volcanic rocks, and clastic and carbonate sedimentary rocks that have been metamorphosed to low-grade greenschist to amphibolite facies. The volcanic rocks have geochemical characteristics consistent with a 'within-plate' or 'island-arc' origin (Zhai and Santosh, 2011). The upper formation is largely composed of detrital rocks, represented by argillaceous schists and siltstones, and marbles (including significant magnesite units), all of which are commonly graphitic (Zhai and Santosh, 2011), but does not appear to include a significant calc-alkaline volcano-plutonic component. Zhai and Santosh (2011) suggested these belts reflect a period of extension/rifting from 2.3 to 2.0 Ga, followed by compression, subduction, collision and accretion from 2.01 to 1.97 Ga. However, instead, Zhao et al. (2012) presented evidence for a progressive closure of these three belts, with the Khondalite and Jiao-Liao-Ji belts closing at ~1.95 Ga to form a Western and Eastern block that straddled the Central Orogenic Belt, before colliding at 1.85 Ga. The latter interpretation is based on the dominance of 1.85 Ga, and almost complete absence of earlier, metamorphic ages in the Central Orogenic Belt (Zhao et al., 2012).

The Khondalite Belt is unusual in that it is characterised by both high-pressure (HP) pelitic granulites and high- to ultra-high temperature (HT to UHT) rocks, although the dominant facies are medium-pressure (MP) pelitic granulites (Zhai and Santosh, 2011; Zhao et al., 2012). The HP pelitic granulites are characterised by the key peak mineral association of kyanite-K feldspar-garnet, in contrast to MP pelitic granulites that have a peak assemblage of sillimanite-K feldspar-garnet (O'Brien and Rotzler, 2003). The pelitic granulite belt is interpreted to be the result of the 2.01 to 1.97 Ga compressional event, culminating in continent-continent collision, overriding of the Yinshan onto the Ordos block, and the consequent deep subduction/imbrication of pelitic sedimentary protoliths to lower crustal depths, generating the MP and then the HP pelitic granulites (Zhao et al., 2012). The HP granulites were metamorphosed at 10 to 13 kbars and 850 ± 50 °C (Li et al., 2000; Kröner et al., 2002, 2005; Zhao et al., 2004). Some crustally derived granitic melts, intruded into the Palaeoproterozoic volcano-sedimentary rocks, were emplaced between 2.05 and 1.99 Ga (Zircon U-Pb; Geng et al., 2000; Yu et al., 2004).

Petrologic studies indicate that, subsequent to peak metamorphism, there was a temporal transition from HP to HT-UHT granulites that follows a common isothermal decompression history, and corresponds to a rapid exhumation from lowermost-lower to lower-middle crustal levels at ~1.92 Ga (Zhai and Santosh, 2011). However, while the exhumation decreases pressure, the HT to UHT metamorphism can be shown to have occurred at increasing temperatures of 800 to 850 °C and 900 to >1000 °C respectively (Zhai and Santosh, 2011). These relationships are taken to imply that the UHT rocks in the Khondalite Belt may have formed in a different tectonic setting to that of the MP and HP granulites. Zhai and Santosh (2011) and Zhao et al. (2012) suggested the HT to UHT metamorphism was related to high temperature gradients of 22 to 28 °C/km (compared to the 16 to 22 °C/km for the HP granulites). They also suggested this might be brought about by underplating and intrusion of large volumes of high temperature mantle-derived magmas during post-collisional extension. This may be caused by mantle inflow and decompression melting, following either slab break-off and detachment, or delamination and detachment of tectonically thickened lithospheric mantle. The interpreted mantle derived deep magma bodies may be reflected by the meta-gabbro dykes which intrude the UHT granulites, and have been dated at 1927 ± 12 Ma (SHRIMP U-Pb zircon; Zhao et al., 2012). Similar MP to HP and HT to UHT granulites also occur extensively in the Central Orogenic and Jiao-Liao-Ji belts (Zhai and Santosh, 2011).

Within these orogenic belts and the neighbouring blocks, extension and continued uplift of the crystalline basement to upper crustal levels between 1.86 and 1.70 Ga, was accompanied by partial melting of the lower crust under the influence of mantle-related underplating/intrusion, with attendant regional metamorphism (1.86 to 1.83 Ga granulites, and 1.80 to 1.79 Ga amphibolites), migmatisation (~1.80 Ga), closely followed by the emplacement of regional scale mafic dyke swarms (1.80 to 1.76 Ga), the development of intra-continental rifting (between 1.85 and 1.70 Ga) and anorogenic magmatic intrusions (1.78 to 1.68 Ga), which included rapakivi granites, anorthosites, gabbros, ultramafic bodies, isolated granites and pegmatites (Kusky and Li, 2003; Kusky et al., 2007a; Zhai and Santosh, 2011).

This tectono-thermal regime led to the development of a network of intra-continental rift basins over and along the margins of the craton, while mafic dyke swarms were emplaced on a large scale over areas of thousands of square kilometres between the rift zones. These rifts are found along the northern margin of the craton, over parts of the Alashan Block, around the western, southern and eastern rim of the Ordos Block, and distributed obliquely across the Central Orogenic Belt. The sequence within these basins varies, but generally comprises voluminous felsic volcanic magmatism and late Palaeo- to early Mesoproterozoic sequences of conglomerates and quartzites, grading upwards into shales and shallow marine carbonates in the upper, thermal subsidence sag phase, reaching a peak at ~1.6 Ga and continuing until ~1.4 Ga (Kusky et al., 2007a). At Bayan Obo, for example, on the northern margin of the North China Craton, sometime between 1.86 and 1.5 Ga, a ~2 km thick rift fill sequence is cut by 1426 ± 40 Ma (Sm-Nd mineral age) carbonatite dykes (Nakai et al., 1989; Le Bas et al., 1992; Fan et al., 2002; Kusky et al., 2007b). Zhai and Santosh (2011) suggested post-1.85 Ga thermal metamorphism, rifting, mafic dyke swarms, magmatism and interpreted underplating, are the result of plume clusters that contributed to the break-up of Columbia, and includes a number of triple points concentrating both rifting and magmatism.

The progressive amalgamation of the Archaean and Palaeoproterozoic micro-continental blocks to form the Western and Eastern blocks, and then a single craton, as described above, are taken to be part of the global orogenic event that culminated in assembly of the Columbia supercontinent by ~1.85 Ga (Kusky et al., 2007b). The subsequent onset of extensional tectonics presaged the global breakup of Columbia, that continued until ~1.4 Ga (Kusky and Santosh, 2009). In the western half of the North China Craton, the break-up of Columbia only seems to have affected the northern margin of the currently preserved craton. Along this margin, a major fault marks the boundary with accreted lower Palaeozoic arc related rocks of the Central Asian Orogenic Belt. Inboard of this fault, the Archaean basement is overlain by a late Palaeoproterozoic intracratonic rift sequence that grades northward into a deeper water facies. These sequences are locally overlain by Neoproterozoic to early Palaeozoic passive margin sediments, intruded by late Palaeozoic granitic and ultramafic rocks and overlain by Carboniferous–Permian strata. These relationships

suggest that either a northern extension of the North China Craton separated along the intracratonic rift core at ~1.4 Ga to create a passive margin through to the lower Palaeozoic, or a passive margin has existed there since the Palaeoproterozoic. In contrast, the southwestern margin of the craton, shared with the Qilian Orogen, does not appear to have opened until the late Neoproterozoic, as detailed below, and remained interior to both the Columbia and subsequent Rodinia supercontinents until the break-up of the latter.

2.1.3. Alashan Massif

The Jinchuan mafic-ultramafic intrusion is located within the Alashan Massif (the Archaean Alashan Block), the westernmost section of the North China Craton, which occupies the western half of the Palaeoproterozoic Yinshan Block (Fig. 1). Mesozoic and Cenozoic cover largely conceal the Yinshan Block, and pre-Neoproterozoic crystalline basement rocks are only exposed in its southwestern and eastern parts. The rocks in the eastern section, to the east of the Alashan Massif boundary, comprise orthogneisses and metasedimentary rocks (with 3.5 to 2.5 Ga detrital zircons), supracrustal metabasic rocks (amphibolites and mafic granulites), metamorphosed intermediate to acid volcanic rocks and abundant granitoids, all of which are dated at ~2.59 to 2.50 Ga. Unlike most of the other Archaean micro-continental blocks of the North China Craton, it does not contain well developed quartz-magnetite/banded iron formations (Yang et al., 1988; Geng et al., 2006).

Within that part of the Yinshan Block occupied by the Alashan Massif, the two oldest complexes, located in the east of the massif, are mainly composed of metamorphic rocks with mafic and felsic protoliths. The primary magmatic ages of the mafic and felsic igneous rocks are ~2.34 Ga and ~2.32 to 2.30 Ga (SIMS U-Pb zircon), respectively. Both sets of rocks were intruded by granites dated at ~1.98 to 1.97 Ga, and overprinted by two metamorphic events at ~1.89 and ~1.79 Ga (Dan et al., 2012). Geochemical and zircon Hf-O isotopic data indicate the ~2.34 Ga amphibolites are consistent with continental rift basaltic rocks. Similar data suggest the ~2.32 to 2.30 Ga felsic rocks were generated by re-melting of dominantly meta-igneous rocks that have zircon Hf model ages of 2.92 to 2.81 Ga (Wan et al., 2001). These zircon Hf model ages differ from those of ~2.8 to 2.6 Ga for the majority of igneous rocks from elsewhere in the North China Craton. These complexes in the east have a southwest structural grain, parallel to the margin of the Khondalite Belt, with an arcuate westward transition to northwesterly trends along the southwestern margin of the massif.

The Longshoushan Terrane, in which the Neoproterozoic Jinchuan intrusion is located, is in the southwestern Alashan Massif, and has a northwest trend, parallel to the current craton margin. It is a Cenozoic uplift, surrounded by Mesozoic to Cenozoic cover, which exposes amphibolite to granulite facies metamorphosed igneous rocks formed between ~2.1 and 2.0 Ga, unconformably overlain by greenschist-facies meta-sedimentary rocks of >1.72 Ga age (Tung et al., 2007 and references therein; Dan et al., 2012 and references therein). These interpretations are supported by SHRIMP U-Pb detrital zircon dates by Tung et al. (2007) which were dominantly 2.2 to 1.7 Ga, with a peak at 2.0 to 1.8 Ga, a smaller group (~20%) at 2.7 to 2.3 Ga, whilst the youngest was 1724 ± 19 Ma. Neoproterozoic rift type sedimentary rocks unconformably overlie the two Palaeoproterozoic sequences.

The pre-Neoproterozoic sequence within the Longshoushan Terrane constitutes the Longshoushan Group, which is as follows, from the base, after Tang (1993) and Tung et al. (2007):

- *Qilingou Formation*, the lowest member of the group, which is not exposed in the immediate Jinchuan district. It is composed of banded augen migmatites, interfoliated with plagioclase amphibolite gneiss, and thinly-bedded and serpentinised marble, which have been metamorphosed to grades ranging from granulite to lower-amphibolite facies, and represent a sequence of sedimentary protoliths overlain by intermediate to mafic volcanic rocks.
- *Baijiazui Formation*, which is largely found in the middle segment of the Longshoushan Terrane, including the Jinchuan district. It is mainly composed of interbedded marble and biotite gneiss, garnet bearing two-mica quartz schist and plagioclase amphibolite, and has been metamorphosed to lower-amphibolite facies from protoliths that comprised a lower Mg-rich marble unit overlain by marine clastic rocks. In the Jinchuan area it includes significant migmatites, and may include rocks mapped elsewhere as Qilingou Formation. The formation has a total thickness of >3500 m.
- *Tamazigou Formation*, which occurs throughout the terrane, and unconformably to disconformably, overlies the Baijiazui Formation. It is primarily composed of two-mica quartz schist, plagioclase amphibolite, plagioclase leuco-leptite, minor marble, dolomite, biotite-plagioclase gneiss and quartzite, and has been metamorphosed to upper greenschist facies from a sequence that progressed from flyschoid protoliths to an upper suite of marine carbonate rocks.
- *Shijingkuo Formation*, which is largely found in the northwest of the terrane. It consists of a lower sequence of leuco-leptite, quartzite and metadacite, a middle mica-quartz schist and gneiss, and upper leptite gneiss and crystalline limestone. The sequence has mainly been metamorphosed to lower greenschist facies, from protoliths that commenced with continental clastic rocks, overlain by a marine volcano-sedimentary package.

The Qilingou and Baijiazui formations represent the ~2.1 and 2.0 Ga sequence, and the Tamazigou Formation the part of the succession that was deposited between ~1.85 and ~1.72 Ma. These ages are supported by observations that the Baijiazui Formation is cut by an ~2 Ga granitic dyke (U-Pb zircon; Tang and Li, 1995a,b), and the Tamazigou Formation by a 1719 Ma white pegmatitic granite dyke (Tang, 1993). The Shijingkuo Formation may extend into the Mesoproterozoic.

The Alashan Massif differs from the eastern Yinshan Block and the Archaean micro-continental blocks elsewhere in the North China Craton, in that it is only composed of Palaeoproterozoic rocks, although an underlying Archaean basement is suggested in the remelted meta-igneous source of the felsic magmatic rocks. The sequence is broadly comparable with the Khondalite Belt in that both comprise a lower bimodal volcanic suite deposited between 2.3 and 1.9 Ga, overlain by a succession of clastic and carbonate sedimentary rocks, with lesser volcanic lithologies. Both the Khondalite Belt and Alashan Massif are overprinted by two metamorphic events (Alashan Massif ~1.89 and ~1.79 Ga; and Khondalite Belt 1.86–1.83 and 1.80–1.79 Ga), which are not precisely of the same age, although the Alashan Massif has not been subjected to the ~1.92 Ga HP and HT to UHT conditions characteristic of the Khondalite Belt. It is therefore reasonable to suggest that Alashan Massif may represent an equivalent sequence to that in the Khondalite Belt, but that it has remained external to the structural zone that has produced the extreme tectonic and metamorphic influences imposed on the latter. The upper, post 1.85 Ga Tamazigou and Shijingkuo formations in the Longshoushan Terrane would appear to represent deposition within, or lateral to, a late Palaeoproterozoic intra-cratonic rift zone as recorded elsewhere throughout the North China Craton.

Some authors (e.g., Zhang et al., 2011; Song et al., 2012c; Cocks and Torsvik, 2013) argued that the Alashan Massif is not part of the

North China Craton, but instead is related to the Qilian-Qaidam complex, Tarim Micro-continent and Yangtze Craton. This conclusion is based on the differences in the age of exposed basement, as discussed above, the predominance of Palaeoproterozoic lithologies and the marginal differences in ages of deformation. Zhang et al. (2011) also observed the absence of zircons derived from the Ordos Block in Ordovician sedimentary rocks of a foreland basin that overlapped the Qilian Orogen and Alashan Massif during their early Palaeozoic collision. They suggest this shows that the Alashan Massif did not collide with the North China Craton until after the Ordovician. If the Alashan Massif were separate from the North China Craton until the early Palaeozoic or later, it would have implications for the interpretation of the Palaeoproterozoic history of the craton outlined herein. It would also require a major suture zone, as yet not reported.

2.2. Tarim micro-continent

The Tarim Micro-continent (Fig. 1) has an almond-shape, covered by a thick (up to 15 km), and poorly deformed, succession of Neoproterozoic to Cenozoic strata. This sedimentary basin largely conceals an Archaean to Palaeoproterozoic basement of TTG gneisses and amphibolites that are only locally exposed at a few sites on the rim of the cover basin (Xu et al., 2005b, 2009; Zhang et al., 2007a; Lu et al., 2008). The micro-continent is separated from the northwestern margin of the North China Craton (~150 km north of Jinchuan) and from the Qilian and Qaidam blocks by the major east-west Altyn Tagh fault system, a multi-strand strike-slip shear zone that is ~100 km wide. Cenozoic (post 55 Ma) sinistral displacement on this structure is estimated at 475 ± 70 km, related to closure of the Tethys Sea and advance of the Indian plate from the south (Cowgill et al., 2003).

Archaean rocks, predominantly garnet gneisses, granitic gneisses and ferruginous quartzites, are only exposed on the eastern and northern margins of the craton, whilst unconformably overlying Palaeoproterozoic high-grade metamorphic rocks and Mesoproterozoic lower-grade metamorphic strata are widespread. In this sense, the Tarim Micro-continent resembles the tectonically juxtaposed Alashan Massif. The Palaeoproterozoic sequence includes biotite-quartz-schist, biotite-schist, marble, hornblende-schist, sericite-schist and granitic rocks with a spilitic volcanic suite. The basal units of the unconformably overlying Tarim Basin sequence comprise post 850 Ma Neoproterozoic rocks, which include the well-preserved glacial event sequences of this period (Lee, 1985; Lu et al., 2008). Late Mesoproterozoic to mid-Neoproterozoic tectono-thermal events fall into two periods, the late 'Grenvillean' 1.05 to 0.90 Ga event, which is similar to that of the Yangtze Craton Yangtze Craton (but not the Alashan Massif), and reflects a compressive regime corresponding to the final assembly of Rodinia. The second is a rifting phase that lasted from 820 to 740 Ma, similar to that in the Alashan Massif (Lu et al., 2008).

Geophysical and drilling data suggest that the underlying micro-continent is composed of a northern block, which contains both Archaean and Palaeoproterozoic basement with an east-west grain in magnetic data, and a South Tarim basement, which is only of Palaeoproterozoic age, and has a northeast trending magnetic trend. These two domains are separated by an ~1100 km long by 60 to 80 km wide, east-west trending, high positive magnetic anomaly belt, which chiefly consists of basic to ultrabasic plutonic rocks, probably representing a suture zone (Lee, 1985; Guo et al., 2001). As there is no change in the character of the overlying Cambrian and younger stratigraphy across both blocks, the two are interpreted to have been amalgamated during the Proterozoic, which Guo et al. (2001) suggested was after 800 Ma, as the Sinian (800 to 570 Ma) part of the cover sequence, which is mapped conformably above the North Tarim Block, is absent over the South Tarim Block.

2.3. Qilian and Qaidam blocks

The Qilian and Qaidam basement blocks (Fig. 1) are micro-continental slivers that collided with the North China Craton during the lower Palaeozoic. They both include 2.4 to 1.8 Ga Palaeoproterozoic basement rocks and have been regarded as being extensions of the Tarim micro-continent, offset across the Cenozoic Altyn Tagh fault zone (Song et al., 2012c). They are separated by the lower Palaeozoic North Qaidam orogenic belt of ultra-high pressure (UHP) metamorphic rocks, whilst the Qilian Block is separated from the southwestern margin of the North China Craton (including both the Alashan Massif and Ordos Block) by the lower Palaeozoic Qilian Orogen.

The Qaidam Block basement is concealed by the thick (up to 15 km) Cenozoic cratonic succession of the internal drainage Qaidam Basin (Zhu et al., 2006). It comprises metamorphic rocks that include eclogites, mélange, shallow marine strata and turbidite protoliths, intruded by granitoids (Gehrels et al., 2003) that have yielded ages of 794, 1120 and 1474 Ma (RGST-QBMG, 1986). The same plutons were subsequently largely dated at 425 Ma by Gehrels et al. (2003), although the latter researcher did obtain one set of ~930 to 920 Ma ages confirming the Proterozoic age of the block.

Much of the crust in the Qilian Block appears to have been assembled prior to 930 to 920 Ma granitoid intrusion, and largely comprises slices of oceanic crust, thick piles of turbidites and sequences of shallow marine strata (Gehrels et al., 2003). There is some uncertainty as to how much of the Qilian Block is Proterozoic, but it does include a narrow band of Palaeoproterozoic metamorphic rocks (the Oulongbuluk sub-block containing granitic gneiss and amphibolite with 2412 ± 14 Ma and 2366 ± 10 Ma ages, respectively; Lu et al., 2002). Some of the mylonitic and metamorphic rocks on its northern margin and within the Qilian Orogen, previously thought to be Proterozoic, are of Palaeozoic age (Xiao et al., 2009).

No Archaean basement has apparently been recognised to the south of the Altyn Tagh fault, which may in part follow a reactivated, much older structure (Guo et al., 2001). The same authors suggest the South Tarim and Qaidam blocks were amalgamated between 1.5 and 1.4 Ga, across a suture that closely follows the Altyn Tagh fault zone, prior to collision with the North Tarim block in the Neoproterozoic. However, Gehrels et al. (2003) indicated the shallow marine sedimentary sequences and metaturbidites in the Qilian and Qaidam blocks yield detrital zircon ages that are quite unlike the ages of igneous rocks in the Tarim and North China cratonic rocks, and may have been accreted to the South Tarim block later than envisaged by Guo et al. (2001). Song et al., 2012c noted ~1000 to 900 Ma granitic gneisses, intrusions and metapelites belonging to the Qaidam Block thrust into the North Qaidam UHP metamorphic belt, which they suggest indicate late 'Grenville-age' juvenile crustal accretion protoliths during formation of the Rodinia Supercontinent, indicating proximity of the Qaidam Block to the margin of that supercontinent.

2.4. Rodinia break-up and mafic intrusions

The sequence of events and relationships outlined above suggest that from ~1.9 Ga, the area of the preserved western North China Craton (including the Alashan Massif) remained within a larger block that was towards (200 to 250 km from) the northern margin of the Columbia supercontinent. This same area was little affected by the breakup of the supercontinent elsewhere, other

than intra-cratonic extension, mafic underplating and anorogenic magmatism, and became part of the subsequent Rodinia supercontinent, which, on a global scale, was progressively assembled between 1300 and 900 Ma. According to Li et al. (2008) and other authors, the collision and coalescence of virtually all known continental blocks into Rodinia, led to a cessation of most subduction and mid-ocean spreading, and the detachment of stagnated slabs, which accumulated at the mantle transition zone below the supercontinent. This latter process produced mantle avalanches, which in conjunction with the thermal insulation of the supercontinent, led to the formation of a number of clusters of mantle superswells (or superplumes) beneath different parts of Rodinia, ~40 to 60 Myr after its assembly. As a result, widespread intracontinental fracturing and rifting occurred between ~880 and 740 Ma, with episodic plume events at ~880, ~820, ~780 and ~750 Ma. These plume events resulted in one or more of the following over areas of several hundred thousand square kilometres: (i) updoming and radial fracturing, (ii) intracratonic rift zones, (iii) mafic dyke swarms, (iv) layered mafic intrusions, (v) widespread anatectic granitoid plutonism and (vi) bimodal volcanic flow provinces. The first major continental separations occurred possibly as early as 750 Ma. Most of the intracratonic rift zones did not progress to breakup, although some did continue opening, to become oceanic basins, and formed new oceans behind separated continental and micro-continental blocks. By 530 Ma, a suite of new continents, micro-continents and cratonic slivers had split from Rodinia, and had begun to re-amalgamate in a different permutation to form the new, but short-lived supercontinent, Pannotia.

The breakup of Rodinia eventually led to the fragmentation of the larger continental mass that had enclosed the currently preserved North China Craton. The western section of the craton that hosts the Jinchuan ultramafic intrusion, broke along a southeast trending line to the southwest of the deposit, that intersects with the northern margin of the craton ~300 km to the northwest (Fig. 1). The early stages of breakup appear to have taken the form of southeast trending faulting, that provided pathways for a >75 km long corridor of >100 km, elongate, ultramafic intrusions, which include both sulphide-mineralised (e.g., Jinchuan, Zhangbutai and Qingjingzi; Fig. 2) and barren bodies (e.g., Qingshiyao, Xijing, Maocaoquan and Dongwan; Chen et al., 2013). The Jinchuan intrusion, which is ~6500 m long and a few, up to 500 m wide, dips at 50° to 80°SW, and is composed of dunite, lherzolite and pyroxenite, and has an indicated crystallisation age of 827 ± 8 Ma (U-Pb SHRIMP dating of zircon and baddeleyite; Li et al., 2004, 2005). The other intrusions of the corridor are generally smaller, e.g., Zhangbutai, which is composed of lherzolite and pyroxenite, is 2500 m × 120 m to 2500 m × 370 m; whilst Qingshiyao, which is dominantly composed of pyroxenite, is 1300 m × <110 m. Other

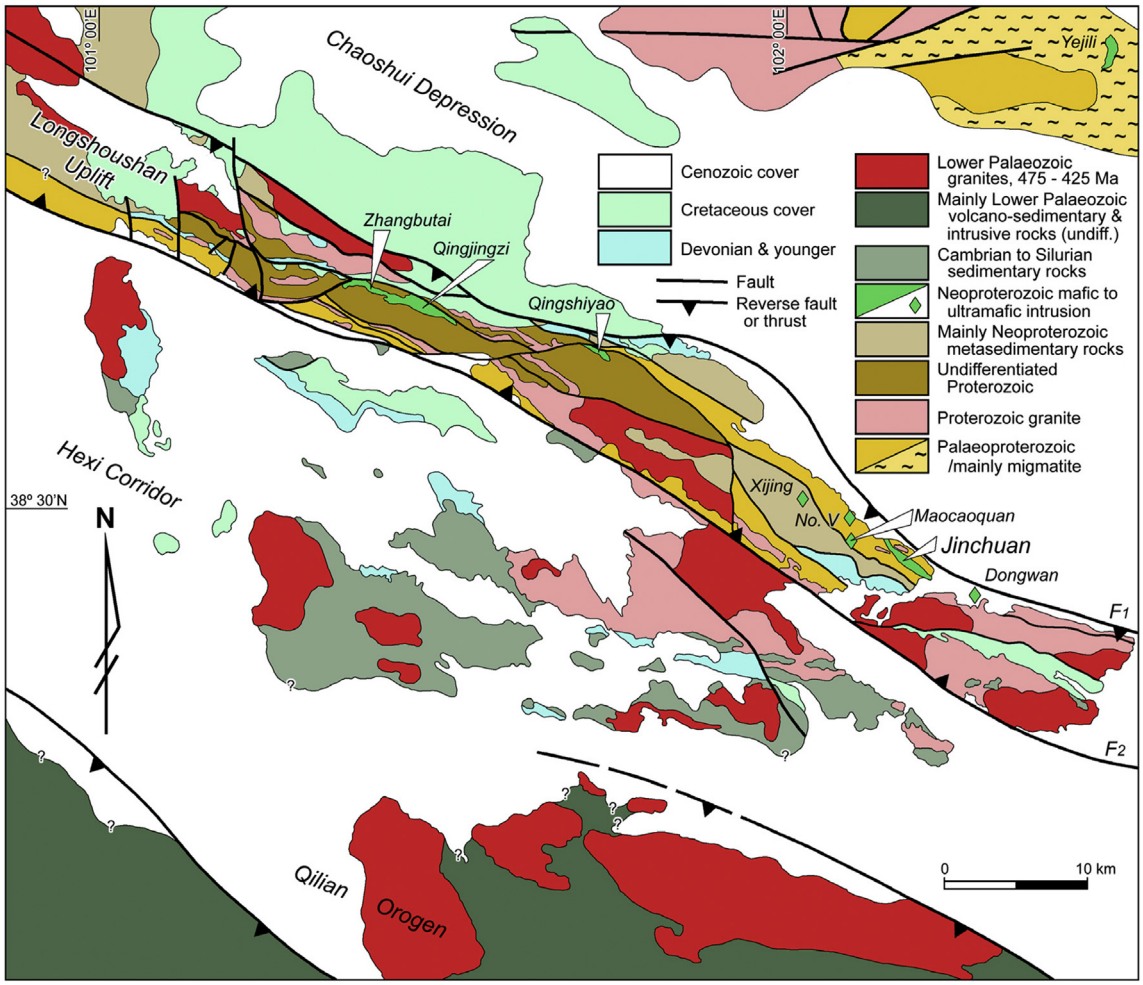

Figure 2. Geology setting and structure of the Longshoushan Uplift and location of the Jinchuan ultramafic intrusion. Composite map after the following: The geology of the main Longshoushan Uplift after Li et al. (2004) and Song et al. (2012a,b); northeast of the Chaoshui Depression after Li et al. (2004); Hexi corridor geology after Song et al. (2012a,b) and structures after Champagnac et al. (2010); Qilian Orogen after Xu et al. (2005a), Xiao et al. (2009); granitic intrusion outlines and ages after Huang et al. (2014).

similarly elongated ultramafic bodies are also found elsewhere, e.g., the barren Yejili intrusion, 65 km to the northeast of Jinchuan (Fig. 2), is 6500 m long × 800 m wide, and mainly comprises plagioclase peridotite with a discontinuous margin of clinopyroxene peridotite (Barnes and Tang, 1999).

The Jinchuan Ni-Cu-PGE sulphide-bearing intrusion, along with related coeval regional mafic dykes and tholeiites, as well as other mineralised mafic-ultramafic complexes, are interpreted by Li et al. (2005) to be genetically related to a mantle plume. The same authors suggest that the integrated mineralogical, petrological and geochemical data (e.g., REE and MgO compositions) are all consistent with the presence of a mantle plume with a potential temperature (T_p) of >1350 °C, and that the Jinchuan parental magma was generated by high degree melting of the sub-crustal lithospheric mantle (SCLM) heated by an anomalously hot, mantle plume.

Chai and Naldrett (1992) suggested that the parental magma of the Jinchuan intrusion was a high-Mg basalt formed by high degree melting of the mantle. However, Li et al. (2005) demonstrated that the Os isotopic composition of the magma is not consistent with values of any known mantle reservoirs and that the only probable source of the parental magma was most likely derived from a long-term enriched SCLM source, as stated above. Li et al. (2005) also concluded that the Jinchuan mafic-ultramafic rocks share a geochemical affinity with similar intrusions of the Yangtze Craton, on the basis of SHRIMP U-Pb ages of both baddeleyites and zircons of igneous and inherited origin, but are also coeval with the interpreted ~825 Ma plume-related mafic dykes, tholeiites and mafic-ultramafic complexes with associated V-Ti and Ni-Cu-PGE mineralisation found within that craton. The same authors therefore consider it likely that the Yangtze Craton was rifted from the southwest margin of the North China Craton following emplacement of the Jinchuan ultramafic intrusion. However, much of the Yangtze Craton was affected by the 'Grenville' aged orogeny, which marked the active accretionary margin of Rodinia during its assembly. Similar Grenvillean activity is not characteristic of the North China Craton. Consequently, if the Yangtze Craton separated from the North China Craton along a break to the southwest of Jinchuan, it would mean that this break was distal to the margin of Rodinia, which would have been on the opposite margin of the newly formed Yangtze Craton. In addition, as interpreted plume-related magmatism is restricted to the preserved western North China Craton (Alashan Massif), and if reflecting the same plume cluster that influences much of the Yangtze Craton, the centre of the system would have been to the west, along the strike of the corridor of mafic to ultramafic intrusions at Jinchuan.

The ultramafic intrusions at Jinchuan are hosted within a Palaeoproterozoic sequence, exposed in the northwest striking, ~200 km × 20 km, Longshoushan Terrane, to the northeast of the Qilian Orogen. This terrane is a Cenozoic uplift, bounded to the northeast and southwest by inward dipping (60° to 70°) reverse faults that are still active. The northern of these structures overlies >2700 m of Mesozoic and Cenozoic strata and represents uplift of >4 km, where the Palaeoproterozoic Baijiazui Formation is juxtaposed with post-Palaeozoic rocks. The sequence within the terrane belongs to the Longshoushan Group, as described above in the *Alashan Massif* Section 2.1.2. This sequence is unconformably overlain by a rift sequence of Neoproterozoic conglomerate, sandstone and crystalline limestone, and unconformably overlying late Neoproterozoic to Palaeozoic sericitic quartz schist, calcareous schist and limestones (Tang, 1993). The Neoproterozoic rift sequences are most likely a further reflection of early extension related to the pending Rodinia breakup. The ultramafic intrusions are restricted to the Palaeoproterozoic metamorphic rocks (Song et al, 2012a,b), which are unconformably overlain by the Neoproterozoic and Paleozoic strata (Song et al, 2012a,b). Lehmann et al. (2007) noted that the ultramafic intrusions are currently only a few kilometres from the disconformity at the base of the Neoproterozoic cover sequence, and although this separation may have been reduced during subsequent deformation, the change may not have been great. The implication they draw from this observation is that the intrusion may have been emplaced in the upper crust and brought close the surface by erosion and uplift, rather than in the middle to lower crust. The same authors also observe that the emplacement of the intrusion could have taken place before, during, or after deposition of the Neoproterozoic cover sequence, but occurred before the greenschist-facies metamorphic event, which affects both the cover sequence and the intrusion itself, and deformed its margins.

The affects of the Rodinia break-up are also recorded from the Qaidam-Qilian complex to the south of the North China Craton, where fault blocks of Proterozoic basement are exposed within the lower Palaeozoic subduction complex in the northern Qilian Orogen. Early magmatism in this basement is represented by a 1309 Ma package of flood basalts in the Northern Qilian Mountains (Xu et al., 2005a). This magmatism, in conjunction with the ~1000 to 900 Ma granitic gneisses and metapelites on the margin of the Qaidam block, as detailed above, are interpreted by Song et al. (2012c) to indicate Grenville-age magmatism, similar to that in the Tarim and Yangtze cratons, but in contrast to the North China Craton, suggesting the Qaidam-Qilian blocks were not split from the North China Craton during the break-up of Rodinia. Within the North Qilian Orogen, the commencement of the Rodinia break-up is reflected by late Neoproterozoic to early Cambrian continental volcanism overlying basement blocks, beginning with large bimodal volcanic domes, effusive and explosive volcanism, and shallow intrusive activity, as well as fissure-type flow banded lavas. The domes are dominantly alkali basalts, with acid volcanic rocks in the central and lower sections (Xu et al., 2005a). Eclogites within the UHP metamorphic rocks of the North Qaidam Orogenic Belt, similar to those characteristics of the adjacent Qaidam Block, have been dated at ~850 Ma, and interpreted to represent continental flood basalt protoliths (Song et al., 2012c). These rocks have the geochemical features of enriched-type mid-ocean ridge basalts (E-MORB) and oceanic island basalts (OIB), and Ti:Y patterns characteristic of flood basalts such as the Permian Emeishan basalts in southern China (Xu et al., 2001; Song et al., 2012c).

By the late Cambrian, breakup was well advanced, having progressed from intracontinental rift to oceanic basin, with 522 to 495 Ma mid-ocean ridge rocks, now preserved as obducted slices in the North Qilian Mountains (Xu et al., 2005a). These rocks have low-K tholeiite, and ocean island alkali and tholeiitic series compositions, and E-MORB and T-MORB features (Xia et al., 1998; Ge and Liu, 1999; Zhang et al., 2000). Although preserved in the Qaidam-Qilian complex, these rocks represent oceanic crust that separated the Qilian Block and North China Craton prior to the lower Palaeozoic subduction that brought the two tectonic elements together. The break-up may have opened an ocean of >1000 km width.

2.5. Qilian and North Qaidam orogenic belts

During the break-up of Rodinia, the cratonic elements that separated from the southern margin of the North China Craton were rifted away by the intervening ocean that formed. By 486 Ma, the oceanic plate had cooled, extension had been reversed to compression, with a different vector of motion, and the Tarim Micro-continent, and the Qaidam and Qilian blocks/fragments, approached the western North China Craton from the southwest (Xu et al., 2005a; Du et al., 2007). Their progressive collision and

amalgamation produced both the North Qaidam ultra-high pressure (UHP) metamorphic belt and the complex Qilian Orogen (Fig. 1). Both the Qilian and North Qaidam orogenic belts are marked by lower Palaeozoic suture zones (Song et al., 2009a, 2012c).

The Qilian Orogen (Fig. 1) extends over a strike length of >1000 km, is > 150 km wide, and separates the North China Craton from the Qilian Block. Its current northern margin passes within 25 km to the southwest of the Jinchuan ultramafic intrusion. This orogenic belt encloses multiple oceanic-type sutures, resulting from the collision and telescoping of at least three intra-oceanic and oceanic-cratonic subduction zones of opposing polarity (Xiao et al., 2009). It includes subduction complexes, ophiolitic mélanges, high-pressure blueschist eclogites, back-arc sequences and Ordovician to Silurian volcano-plutonic arc rocks, mainly basalts to andesites and granitoids, and faulted slivers of Proterozoic basement. While the main subduction activity was located to the south, lower Palaeozoic foreland basins extended onto the North China Craton to overlap the Jinchuan district, filled with Cambrian to Silurian sedimentary rocks largely derived from the arcs in the south. This belt was produced by a complex evolution of subduction-accretion processes from the Cambrian, to the final amalgamation and docking of the entire Qilian orogenic collage to the North China Craton in the late Devonian, terminating the intervening ocean. During and following collision, the Qilian Orogen arc rocks were thrust over the North China Craton. The belt reduced to just a foreland basin during the early Devonian, onlapping both the North China Craton and Qilian Orogen, after which, orogenesis migrated southward into the Central China Orogen (Wu et al., 1993; Du et al., 2004; Xu et al., 2005a; Song et al., 2007, 2009a,b; Zhang et al., 2007a,b; Xiao et al., 2009).

In contrast, the North Qaidam ultra-high pressure (UHP) metamorphic belt is of a continental-type, characterised by UHP eclogite-facies blocks and lenses hosted in UHP granitic gneisses, comprising granitic and pelitic gneisses, eclogites and garnet peridotites. These assemblages are interpreted to result from the Qaidam and Qilian continental crust plates colliding and overthrusting following subduction of intervening oceanic crust. Between ~460 and 420 Ma, continued compression resulted in imbrication, and the Qaidam continental crust plate was pushed below the Qilian Block to depths of ~100 to 200 km, where it was subjected to HP to UHP metamorphism, before being exhumed in the late Silurian to Devonian (Xiao et al., 2009; Huang et al., 2014).

Granites are abundant within both the Qaidam-Qilian orogenic belts and basement blocks. Most are S- or I-type, with trace element patterns resembling the bulk continental crust composition, and were emplaced at ~475 to 425 Ma, although a small number of intrusions have older ages, including 500 and 800 Ma, while slightly more are 930 to 920 Ma (Gehrels et al., 2003; Huang et al., 2014). The latter intrude both shallow marine strata of the Qilian terrane, as well as into ultramafic rocks of the Qaidam block. Similar aged granitoids are not recognised in either the North China or Tarim cratonic rocks (Gehrels et al., 2003), although Wan et al. (2001) reported some 971 to 845 Ma foliated granite intrusions within the Alashan Massif.

2.6. Central Asian orogenic belt

This orogenic belt (Fig. 1) comprises an ~5000 km long, by ~1000 km wide, E–W trending collage of late Neoproterozoic to early Mesozoic volcano-plutonic arcs and arc related rocks that extends from the Ural Mountains to the Pacific coast. Its southern margin with the North China Craton is ~200 km north of Jinchuan.

Yakubchuk et al. (2012) showed that as the Rodinia supercontinent broke-up in the late Neoproterozoic, a series of cratonic fragments (including the Karakum and Tarim micro-continents, and the North China Craton) detached from the southwestern margin of the supercontinent. These fragments, moved obliquely to the southeast, ahead of an expanding oceanic back-arc basin, away from the remaining, but also diverging Eastern European craton (Baltica), Arctic Shelf and Siberian Craton.

The bulk of the magmatic arcs within the Central Asian Orogenic Belt were formed on the southern margin of the Siberian craton, or between it and the Eastern European craton and as intra-oceanic arcs as the oceanic back-arc basin began to close. During this period of accretion, the North China Craton approached from the southwest, and, during the early Triassic, collided with the accreted orogenic belt that separated it from the Siberia Craton. This involved south-directed subduction beneath the North China Craton from 300 to 250 Ma, followed by collision, marked by the Solonker Suture.

From ~1.4 Ga to the late Neoproterozoic, the Yinshan Block of the North China Craton had a northern passive margin, where Archaean basement, predominantly TTG gneisses and minor mafic igneous rocks, is overlain by a Palaeoproterozoic intracratonic rift sequence of metasedimentary and igneous rocks, succeeded locally by Neoproterozoic to lower Palaeozoic passive margin sedimentary rocks. The latter included Cambrian to middle Ordovician platform carbonates. The craton and overlying passive margin sequences are now largely bounded by a major east-west fault zone. This faulted cratonic margin is separated from the Solonker Suture by a 100 to 250 km width of continental growth that had occurred along the northern margin of the North China Craton, mainly between 555 and 396 Ma. These rocks comprise predominantly Ordovician intra-oceanic arc and associated accretionary complexes, which collided with the passive North China Craton margin in the Ordovician, when south directed subduction then built a craton margin arc (Davis et al., 1996, 2002; Yue et al., 2001; Xiao et al., 2003; de Jong et al., 2006; Peng et al., 2013).

Later, towards the end of the Palaeozoic, as the North China Craton approached the Central Asian Orogenic Belt from the southwest, the south-directed subduction below the craton produced an up to ~200 km wide belt comprising a large volume of late Permian to early Triassic and lesser Carboniferous syncollisional granite plutons (Jia et al., 2004), overlain by Carboniferous to Permian andesites, basalts, dacites, rhyolites and associated tuffs. These younger rocks are developed both over the accreted margin and up to more than 100 km into the craton, in places spanning the entire width of the Yinshan Block (de Jong et al., 2006; Peng et al., 2013). The width of this volcano-plutonic belt within the craton tapers to the west towards the faulted contact with the Tarim Micro-continent, suggesting the latter has substantially overridden the Yinshan Block since the early Mesozoic. Continued convergence during the Triassic and Jurassic caused post-collisional over-thrusting and considerable crustal thickening on the NW margin of the craton (Xiao et al., 2003). Subsequent Mesozoic granitoids, metamorphic core complexes and extensional basins, south of the Solonker suture, in both the Palaeozoic accretionary orogen and over the North China Craton, may be related to post-collisional Jurassic to Cretaceous collapse of the Solonker orogen and plateau (Ritts et al., 2001; Xiao et al., 2003).

2.7. Central China orogen

The Central China Orogen is variously defined by different authors, e.g., Kusky et al. (2007b) suggested it as a broad, composite late Neoproterozoic to Mesozoic orogenic belt along the southwestern margin of the North China Craton, separating the latter from the Yangtze Craton in the southeast, and includes the entire

Qilian-Qaidam complex in the west. Kusky and Santosh (2009) instead showed a narrower zone that includes the Qinling-Dabie Belt separating the North China and Yangtze cratons in the east, passing westward to lie immediately south of the Qilian-Qaidam complex, the interpretation applied herein. According to Ratschbacher et al. (2006), the Qinling-Dabie section of the orogen is composed of three closely spaced sutures. The northernmost is intra-oceanic, and separates the North China Craton from the narrow (~10 km wide) Ordovician Erlangping magmatic arc, which is intruded by Silurian–Devonian arc plutons, and is most likely a continuation of one of the multiple Qilian Orogen sutures. The second is of similar age, and separates the Erlangping arc from a long narrow (~10 to 50 km wide) sliver of Proterozoic rock, the Qinling Micro-continent, that has been deformed by a ~1.0 Ga tectonic event, underwent both 0.8 to 0.7 Ga Neoproterozoic and Silurian to Devonian rifting, and is overlain by Devonian to Permian arc rocks and subduction complexes, all of which have been metamorphosed to granulite facies. The third and southernmost suture is of Triassic age, which is related to upper Palaeozoic magmatism, and separates the Qinling Micro-continent from the Yangtze Craton to the south. The Qinling Micro-continent has a common Precambrian history with the Yangtze Craton, but differing Phanerozoic character. The Yangtze Craton, on the southern fringe of the suture, was subjected to Triassic UHP metamorphism when imbricated and carried to mantle depths (~100 km) before exhumation by sub-horizontal extension and rise of the buoyant UHP rocks later, from the Triassic to present. The Qinling-Dabie zone is also intruded by voluminous Cretaceous granitoids. The Triassic suture is assumed to continue westward for ~1500 km as the Kunlun Fault, following the Kunlun Shan along the southern margin of the Qaidam Block, to the Altyn Tagh fault (Cowgill et al., 2003; Kusky et al., 2007b).

2.8. Mid-Palaeozoic to Cenozoic tectonics

The early Mesozoic collision between the North China and Yangtze cratons was broadly coeval with the collision between the North China Craton and the Central Asian Orogenic Belt to the north. The Indian Craton approached from the south during the early Tertiary, behind the North and South Qiangtang and Lhasa Blocks to collide with the main Asian mass. The continued northward compression, following docking, led to large scale imbrication, thickening of the crust below the Tibetan Plateau, and redistribution of structural plates from the Himalayan Front to the North China Craton. Crustal thicknesses to the Moho resulting from this imbrication vary from ~53 km at the Himalayan Front to 80–84 km in the Lhasa Block (Fig. 1), and from 68 to 70 km below the North Qiangtang block, 52 to 60 km below the Qaidam Block, 60 to 70 km in the Qilian Orogen, and 48 to 52 km in the Hexi Corridor (Fig. 2) adjacent to the Jinchuan deposit (Gao et al., 1999).

The ENE trending Altyn Tagh Fault, described above, which marks the boundary between the North China Craton and Tarim Micro-continent, is one of the structures that have accommodated structural redistribution. It has a sinistral displacement estimated at 475 ± 70 km (Cowgill et al., 2003). On the western and eastern extremities of the structure, northwest striking corridors of shallow thrust faults absorb much of this displacement. In the northeast, these thrusts are concentrated along the southern margin of the Hexi Corridor, which follows the boundary between the North China Craton and the Qilian Orogen. This thrusting of the latter over the former has resulted in a northeast vergent cumulative thrust shortening of some 300 km (e.g., Chen et al., 1999; Gao et al., 1999; Yin and Harrison, 2000; Tapponnier et al., 1990; 2001; Champagnac et al., 2010). Coeval with this thrusting, the opposing Cenozoic reverse faults which bracket the Longshoushan Terrane (that incorporates the Jinchuan Ultramafic Intrusion), have accommodated shortening by uplifting the terrane by > 4 km (Champagnac et al., 2010; Song et al, 2012a,b). Consequently, whilst the Jinchuan deposit is currently within 25 km of the southwestern margin of the North China Craton, because of the Cenozoic crustal shortening, it is not possible to estimate its relative proximity to the edge of the craton at the time of Rodinia break-up, which could be as much as several hundred kilometres. It is also located ~200 km to the south of what was the passive margin of the craton (and Alashan Massif) at the time of emplacement, although Mesozoic compression has also thrust the Central Asian Orogen rocks over the northern craton margin.

3. District geology

The Jinchuan ultramafic intrusion, which has been dated as Neoproterozoic (827 ± 8 Ma, Li et al., 2005; 833 ± 35 Ma, Yang et al., 2005; 831.8 ± 0.6 Ma, Zhang et al., 2010), is located close to (500 to 1000 m) the northeastern margin of the Longshoushan Terrane (Fig. 2). This terrane, which represents a northwest striking, fault bounded Cenozoic uplift, is located on the southwestern margin of the Alashan Massif and Yinshan Block (Tang and Li, 1995a,b; Zhou et al., 2002a).

The Longshoushan Terrane is separated from the lower Palaeozoic Qilian Orogen to the south by the northwest trending Hexi corridor, where Proterozoic rocks of the North China Craton are overlain by Cambrian to Devonian sedimentary rocks, intruded by lower Palaeozoic (mainly ~475 to 425 Ma) granitoids and masked by Mesozoic and Cenozoic cover. A series of southwest-dipping thrusts along the southern margin of the corridor may have accommodated up to 300 km of northeast vergent over-thrusting of the Qilian Orogen subduction complex rocks onto the North China Craton (Chen et al., 1999; Gao et al., 1999; Yin and Harrison, 2000; Tapponnier et al., 2001; Champagnac et al., 2010). The Longshoushan Terrane uplift is > 100 km long and 10 to 20 km wide. It is bounded by two main, inward dipping reverse faults to the northeast and southwest respectively, each of which has accompanying secondary structures. The northern fault dips to the southwest at >60°, with Proterozoic metamorphic and Palaeozoic sedimentary and granitic rocks in the hanging wall, and >2700 m of Jurassic to recent terrestrial clastic sedimentary rocks in the footwall, indicating the structure is still active (Song et al, 2012a,b).

Rocks within the uplift are of Palaeo-, Meso- and Neoproterozoic, Devonian, Carboniferous, Permian and Jurassic ages. Palaeoproterozoic rocks are distributed as northwest-striking belts in the marginal part of the uplift. In the Jinchuan district, they comprise the older, 2.1 to 2.0 Ga *Baijiazuizi Formation*, composed of migmatites, gneisses and serpentinised marbles, and the unconformably to disconformably overlying <1.85 to ~1.72 Ga *Tamazigou Formation* that includes two-mica quartz schist, plagioclase amphibolite, plagioclase leuco-leptite, minor marble, dolomite, biotite-plagioclase gneiss and quartzite. Additional Palaeo- and Mesoproterozoic units are represented elsewhere in the Longshoushan Terrane, as described previously (*Alashan Massif* Section 2.1.2), but are not found in the immediate Jinchuan district, where the older sequences are unconformably overlain by a rift sequence of Neoproterozoic conglomerate, sandstone and crystalline limestone of the *Denzigou Formation*, and the unconformably overlying late Neoproterozoic to Palaeozoic sericitic quartz schist, calcareous schist and limestones of the *Hanmushan Group* (Tang, 1993). The Palaeoproterozoic sequences occur as a southwest dipping monocline, unconformably overlain by the Neoproterozoic rift sequence that occupies an anticlinorium. The Palaeozoic, Mesozoic and Cenozoic strata are homoclinal (Tang, 1993).

In addition to the Jinchuan ultramafic intrusion, there are >100 other smaller sulphide-mineralised (e.g., Zangbutai and Qingjingzi) and barren intrusions (e.g., Qingshiyao, Xijing, Maocaoquan and Dongwan) distributed over a 70 km interval of the Longshoushan Terrane as detailed above (*Rodinia Break-up* Section 2.4). Other magmatic activity was also abundant, including late Palaeoproterozoic pegmatitic granite to plagioclase amphibolite (~2.0 and 1.72 Ga; Tang, 1993; Tang and Li, 1995a,b) often occurring as small lenses, which are cut by early Palaeozoic mafic dykes. The most intense magmatism is of lower Palaeozoic age, mainly 515 to 425 Ma, predominantly granitic intrusions of varying size, although minor intrusions of ultramafic rocks, gabbro, dolerite, diorite and granodiorite are also encountered (Tang, 1993; Huang et al., 2014).

4. Deposit geology and mineralisation

The northwest trending, tabular, Jinchuan ultramafic intrusion is ~6500 m long, varies from 20 to ~500 m (averaging 300 m) in width, and persists down-dip for >1100 m. It was emplaced into Palaeoproterozoic metamorphic gneisses, migmatites, schists and marbles of the Baijiazuizi Formation and dips from 50° to 80° to the southwest. The Baijiazuizi Formation metamorphic rocks are cut by granitic and pegmatitic dykes (dated at ~2 Ga by orthite U-Pb; Tang and Li, 1995a,b; Li, 1996) that have not undergone the same degree of metamorphism, which are, in turn, cut by the Jinchuan intrusion, indicating the latter post-dates the high-grade metamorphism (Lehmann et al., 2007). Most of the intrusion outcrops, except at its eastern and western extremities, although at surface it is expressed as a heavily oxidised and rubbly rock (Naldrett, 2004; Chen et al., 2013). The total extent of the intrusion has been delineated by ground magnetic surveys, where it is reflected by a pronounced ~4000 nT anomaly (Jinchuan Mining, pers. comm., 2006).

The following sections describe the key lithologies, ore mineralogy, ore styles and textures, and structure, followed by the detail of how all of these are distributed within the intrusive complex and how they form the three main No. 1, No. 2 and No. 24 orebodies.

4.1. Lithologies

The Jinchuan ultramafic intrusion essentially comprises an olivine-orthopyroxene-chromian spinel (chromite) cumulate, with interstitial phase orthopyroxene, clinopyroxene, plagioclase and phlogopite. On average, the base-metal sulphides, which are predominantly pyrrhotite, pentlandite and chalcopyrite, constitute 5 wt.% of the intrusion (de Waal et al., 2004). It is composed of four main lithologies, as follows (from Naldrett, 2004):

4.1.1. Lherzolite

Lherzolite, locally grading to olivine websterite, is the dominant rock type, comprising ~80% of the Jinchuan ultramafic intrusion. It is essentially an olivine-chromite mesocumulate, containing interstitial pyroxenes, sulphides and minor plagioclase. It is normally massive, with no visible layering, and has a modal composition of 40 to 85% olivine, 10 to 50% pyroxene (predominantly orthopyroxene in olivine-rich phases), and generally <2% plagioclase. Cumulus chromite varies from 0.5 to 2%, whilst there is usually <8 vol.% sulphide, decreasing upwards. The forsterite content of the olivine varies from 82 to 85 mol.% (microprobe analysis; Chai and Naldrett, 1992). The grain size of olivine varies significantly throughout the intrusion, ranging from 0.2 to 8 mm. It is generally, coarse-grained in the core and the lower parts of the intrusion to the west, whereas in the marginal olivine pyroxenite it is usually very fine-grained, ranging from 0.3 to 3 mm, and in the eastern part of the intrusion ranges from 0.5 to 4 mm. The coarse grained olivine usually has irregular margins due to replacement by pyroxene and amphibole, and by serpentine and talc in altered rocks. Medium-grained olivine is commonly rounded and is often enclosed by pyroxene oikocrysts, giving rise to a typical poikilitic texture. Pyroxenes are always interstitial to cumulus olivine, and often replaced by amphibole and chlorite where altered.

4.1.2. Dunite

Dunite usually contains 8 to 30% Ni-Cu sulphides, and has a modal composition of 70 to 90% olivine, 1 to 8% pyroxene (mostly orthopyroxene), generally <1% plagioclase, 1 to 2% chromite and 1 to 3% magnetite, which is mainly associated with the sulphides. Excluding sulphides, this lithology comprises in excess of 90% olivine, and is more accurately termed a sulphide dunite. The forsterite content of the olivine varies from 84 to 85 mol.% (microprobe analysis; Chai and Naldrett, 1992). The orthopyroxene is found as reaction rings surrounding olivine, and is sometimes replaced by clinopyroxene. The chromite is always fine grained (0.01 to 0.02 mm) and euhedral, mainly as inclusions in olivine, although some are interstitial. Sulphides are interstitial, along with pyroxene and plagioclase, and where a pyroxene corona surrounds olivine, the sulphides commonly occur between the silicate aggregates. In extreme cases, dunite may be entirely composed of olivine and interstitial sulphides in a ratio of ~4:1. This rock type ranges from dunite to sulphide-bearing, to sulphide dunite (IUGS classification; Le Maitre et al., 2002), but will be referred to as dunite through the remainder of the paper.

4.1.3. Plagioclase lherzolite

Plagioclase lherzolite acts as an important visible marker layer in the eastern part of the intrusive complex. It contains 3 to 10% plagioclase, which is often saussuritised or chloritised, occurring as an interstitial phase with pyroxene. The average modal composition is 74% olivine, 17% pyroxene and 6% plagioclase. It also contains small amounts of biotite and magnetite, with or without trace sulphides.

4.1.4. Olivine pyroxenite

Olivine pyroxenite comprises <10 vol.% of the Jinchuan ultramafic intrusion. It is composed of 10 to 40% olivine, with the balance being pyroxene, mostly clinopyroxene. The forsterite content of the olivine varies from 79 to 82 mol.% (microprobe analysis; Chai and Naldrett, 1992). The rock has a mesocumulus to orthocumulus texture. Olivine is mostly enclosed by oikocrysts of pyroxene, and is much finer (0.2 to 2 mm) than in the rest of the intrusion. Trace amounts of sulphides are locally present.

4.1.5. Dolerite dykes

In addition to the four main intrusive lithologies, two generations of dolerite dykes are evident within the deposit. Both intrude the marbles. The first is sheared by thrusts, and the second is unsheared and emplaced along the thrusts. Only the unsheared dykes are observed cutting the main Jinchuan intrusion (Lehmann et al., 2007). These authors take this to infer that the main dunite-lherzolite intruded along a first generation dyke, possibly during the intermittent thrusting that sheared it, and was emplaced between the two dyke generations. Zircon from a second generation crosscutting dolerite dyke has been dated at 828 ± 3 Ma (Li et al., 2005). This dyke is composed of 60% plagioclase, 35% pyroxene and 5% amphibole, and has major and trace element chemical compositions characteristic of tholeiitic basalts (Li et al., 2005). In addition to the dolerite, the deposit area is also cut by narrow granodiorite and lamprophyre dykes (Song et al., 2006).

4.2. Ore mineralogy

The principal ore minerals in the Jinchuan ultramafic intrusion include pyrrhotite, pentlandite, chalcopyrite, cubanite, mackinawite and pyrite. Pyrrhotite is the dominant sulphide mineral in the ore. It mainly occurs as 0.1 to 3 mm anhedral or subhedral crystals. Pentlandite is closely associated with pyrrhotite and commonly occurs as 0.12 mm subhedral to euhedral crystals, enclosed by anhedral pyrrhotite. Rarely, exsolution flames of pentlandite are found along boundaries or fractures of pyrrhotite crystals (Naldrett, 2004). Where the ore is altered/oxidised, pentlandite is replaced by very fine violarite, occurring along grain margins or cleavages, and forming a regular network in the pentlandite crystals. This replacement decreases in intensity downward into the deposit, from nearly 50% at the surface, where sulphide ores have been intensely oxidised (Naldrett, 2004).

Chalcopyrite is predominantly found as anhedral assemblages, disseminated within other sulphides, or as very fine veinlets, which crosscut olivine or pyroxene grains, or in small separate copper rich pods. Chalcopyrite is also seen to cut pyrrhotite and pentlandite (Naldrett, 2004). In some massive ore, fragments of pyrrhotite and pentlandite assemblages are enclosed within a chalcopyrite dominant groundmass, suggesting chalcopyrite crystallised later, or was subsequently introduced into the massive ore (Chai and Naldrett, 1992; Naldrett, 2004). Very fine (<<0.05 mm) sulphide droplets (comprising pyrrhotite, pentlandite and chalcopyrite in the ratio of ~7:2:1) are common in cumulus olivine and chromite crystals. This suggests sulphide segregation occurred during olivine and chromite crystallisation and that a significant amount of copper came from the primary sulphide liquid, reflecting a high copper concentration in the original magma (Naldrett, 2004).

Cubanite occurs as a secondary mineral replacing chalcopyrite or pentlandite, generally occurring in small lamellae along the cleavages or fractures of the chalcopyrite or as irregular inclusions in pentlandite. Mackinawite occurs predominantly in pyrrhotite and pentlandite as various irregular replacements (Chai and Naldrett, 1992).

Along with the Co and Ni, a large proportion (>65%) of the Pd of the deposit occurs within pentlandite $(Fe,Ni,Co)_9S_8$ where it is in solid solution, whilst pentlandite and pyrrhotite accommodate significant proportions (~35 to 90%) of the Re, Os, Ru, Rh and Ag. In contrast, chalcopyrite contains a small amount (~10%) of the Ag but negligible platinum-group elements (PGE; Chen et al., 2015). All of the base metal sulphides are devoid of Pt and Ir, which are interpreted to have been scavenged by arsenic to form separate platinum group minerals (PGM) in association with the sulphides during magmatic crystallisation of the intrusion (S.G.U., 1984; Prichard et al., 2013). The dominant PGM is sperrylite $[PtAs_2]$, which occurs as euhedral, 0.005 to 0.2 mm crystals at the boundary of pentlandite, chalcopyrite and pyrite, or within chalcopyrite and cubanite (Chen et al., 2015). A significant proportion of the PGM are associated with a major post-magmatic alteration event (described in the *Post-Magmatic Alteration* Section 4.7, below). PGE were released from the sulphide lattice during alteration, and re-deposited as PGM (Prichard et al., 2013). Froodite $[PdBi_2]$ is an important Pd mineral, which is usually hosted in magnetite formed during the serpentinite-magnetite alteration of base metal sulphides. Moncheite $[(Pt,Pd)(Te,Bi)_2]$, a very common Pt PGM, and Au-bearing PGM, are located in altered silicates. Irarsite [IrAsS] is mainly found enclosed within base metal sulphides, whilst Padmaite [PdBiSe], occurs at the junctions of magnetite and base metal sulphides. Other PGM include native platinum, palladium melonite $[(Ni,Pd,Pt)(Te,Bi)_2]$, michenerite [(Pd,Pt)BiTe] and sudburyite [(Pt,Pd,Ni)Sb] (S.G.U., 1984; Naldrett, 2004; Prichard et al., 2013).

4.3. Ore styles and textures

Five styles of mineralisation are evident in the Jinchuan complex, in decreasing order of importance, net-textured, disseminated and massive sulphides, and copper rich sulphide pods, whilst metasomatic ore is locally found at the contact between marbles and the ultramafic intrusive rocks:

4.3.1. Disseminated

Disseminated, where sulphides, together with other interstitial minerals, are disseminated between olivine grains and are not interconnected. In general, disseminated sulphides represent between 1 and 33 mol.% of the rock (Barnes and Lightfoot, 2005). In most cases at Jinchuan, the sulphide ore occurs as discrete patches in the silicate rocks, and usually contains <1 wt.% Ni. Ore occurs as either small lenses of disseminated sulphides in the upper part of the igneous body, or at both ends and on the flanks of the net-textured ore lens, forming an envelope around it. The disseminated ores have modal contents of <15% base metal sulphides (1 to 8% pyrrhotite, 1 to 5% pentlandite and 1 to 3% chalcopyrite), which are randomly distributed between olivine and clinopyroxene grains (Naldrett, 2004; Barnes and Lightfoot, 2005).

4.3.2. Net-textured ore

Net-textured ore, in which sulphide minerals are interconnected, filling the interstitial voids of the olivine cumulates, and forming a matrix to the silicate minerals. The sulphide content is generally 33 to 66 mol.%, although it can be lower in some cases. At Jinchuan, this is the dominant ore type, with 15 to 40% sulphides and 60 to 85% rounded olivine crystals, containing Ni grades that usually range from 1 to 4 wt.%, with most ~2 wt.%. It has significantly low levels of chalcopyrite (1 to 4%) relative to pentlandite (4 to 10%). Pentlandite occurs as 0.2 to 2 mm subhedral crystals, enclosed within anhedral/subhedral pyrrhotite, or forms aggregates around, or flames within, pyrrhotite. The total pyrrhotite content is 10 to 30%. Chalcopyrite usually occurs as anhedral assemblages, disseminated within the other sulphides, or as very minor veinlets that crosscut silicates.

Net-textured mineralisation commonly occurs as lenses of various sizes in the core or lower part of the sulphide orebodies. The net-textured ore lenses are generally enveloped by disseminated mineralisation across a gradational boundary (Naldrett, 2004; Barnes and Lightfoot, 2005).

High PGE contents (>1 g/t) are common in net-textured ore, with grades that are ~2 to 3 times that of the disseminated ore, and an average Pt concentration of about 0.4 g/t, increasing with depth. PGE enriched lenses are found in both No. 24 and No. 1 orebodies, as detailed in the orebody descriptions below (S.G.U., 1984; Naldrett, 2004).

4.3.3. Massive ores

Massive ores are commonly present within small fractures, and occur as aggregates, or as irregular or lenticular veins, with the same strike as the main orebody, commonly located at its base, grading upward or toward the margin into net-textured and disseminated ore. Massive lenses commonly have a width of ~1 to 5 m, while some smaller (~1 m) ore veins cut other sulphide ores and extend into the country rocks for up to a few metres. They commonly contain >70% sulphides, including 40 to 60% pyrrhotite, 10 to 20% pentlandite and 1 to 7% chalcopyrite (Chen et al., 2013). Pyrrhotite and pentlandite often form a banded texture, accompanied by disseminated chalcopyrite and magnetite. Where this banding is observed, pentlandite is elongated along the banding, and many fractures, which are mostly filled with magnetite veins, are perpendicular to the elongation of the crystal. This has been

interpreted to suggest the massive sulphides were formed under stress, and the sulphide melt was flowing during crystallisation (Naldrett, 2004).

Xenoliths of the country rocks (gneisses, dolerite, marbles, net-textures and other sulphide ores) commonly occur within the massive sulphides, being most abundant near the base (>10%), where they occur as the clasts of an ore breccia, also suggesting the massive sulphide was emplaced dynamically (S.G.U., 1984; Naldrett, 2004; Chen et al., 2013). Tang (1993) suggested that because this ore type cuts dolerite dykes and because there is a low degree of idiomorphism, an undeveloped metasomatic texture, and slight alteration of adjacent rocks, they were formed at a late stage, and at relatively low temperatures.

4.3.4. Copper-rich sulphide pods

Copper-rich sulphide pods occur both at the base of the No. 24 Orebody (S.G.U., 1984) and in individual ultramafic intrusions in the Palaeoproterozoic metamorphic rocks beneath the eastern portion of the Western intrusion. These 'bean pod-shaped' bodies are generally several metres thick and tens of metres long, and contain disseminated or net-textured Cu-rich sulphide ores, characterised by relatively high chalcopyrite proportions (2 to 14% chalcopyrite, 5 to 15% pyrrhotite and 1 to 6% pentlandite; Chen et al., 2013).

4.3.5. Metasomatic ore

Metasomatic ore is locally found in the hanging and footwall of the intrusion, at the contact between marble and the igneous rocks, and surrounding marble xenoliths, accounting for less than 2% of the reserves at Jinchuan. It mainly occurs as very irregularly shaped bodies near the margin of the eastern part of No. 24 Orebody. Sulphide is present as irregular veins or aggregates in the carbonate groundmass. Metasomatic orebodies are difficult to define in the intrusion because they are scattered in marble xenoliths and some contact zones. It is characterised by diopside skarn alteration, consisting of diopside and calcite, minor titanite and iddingsite, with pseudomorphs of olivine, and variable amounts of sulphides (up to 10%). Elsewhere, along the contact between the intrusion and marble, major and trace element data reveal considerable modification of the composition of the ultramafic rocks, particularly an increase in Ca and a decrease in Si. Decarbonation of marble liberated CO_2, which penetrated into the intrusion, causing an increase in oxygen fugacity, which in turn, led to the segregation of ore sulphides (Lehmann et al., 2007).

4.4. Sulphur

Externally derived sulphur has been shown to be important in promoting sulphide saturation and precipitation from mafic melts at relatively low pressure in many large magmatic Ni-Cu sulphide deposits (e.g., Grinenko, 1985; Mavrogenes and O'Neill, 1999; Ripley et al., 1999, 2002, 2003; Holzheid and Grove, 2002). However, at Jinchuan and the other nearby mineralised mafic intrusions no sulphide source wall rocks have been recognised. The sulphur contents of wall rocks of the Jinchuan intrusion are <100 ppm and the $\delta^{34}S$ values of the pyrrhotite-pentlandite-chalcopyrite assemblage in the Jinchuan ore deposit are in the range −2 to 8‰, with over 80% of the values between −2 and 2‰, characteristic of mantle-derived sulphur (Ripley et al., 2005).

4.5. Structure

There are four major fault sets that have dislocated the Jinchuan intrusion (Fig. 3):

- NW–SE striking regional and small scale reverse faults, including the major, >60°SW dipping F_1 fault bounding the Longshoushan Terrane, some 500 to 1400 m northeast of the deposit;
- ENE–WSW striking sinistral strike-slip faults that dip steeply (>70°) to the southeast, and divide the Jinchuan intrusion into

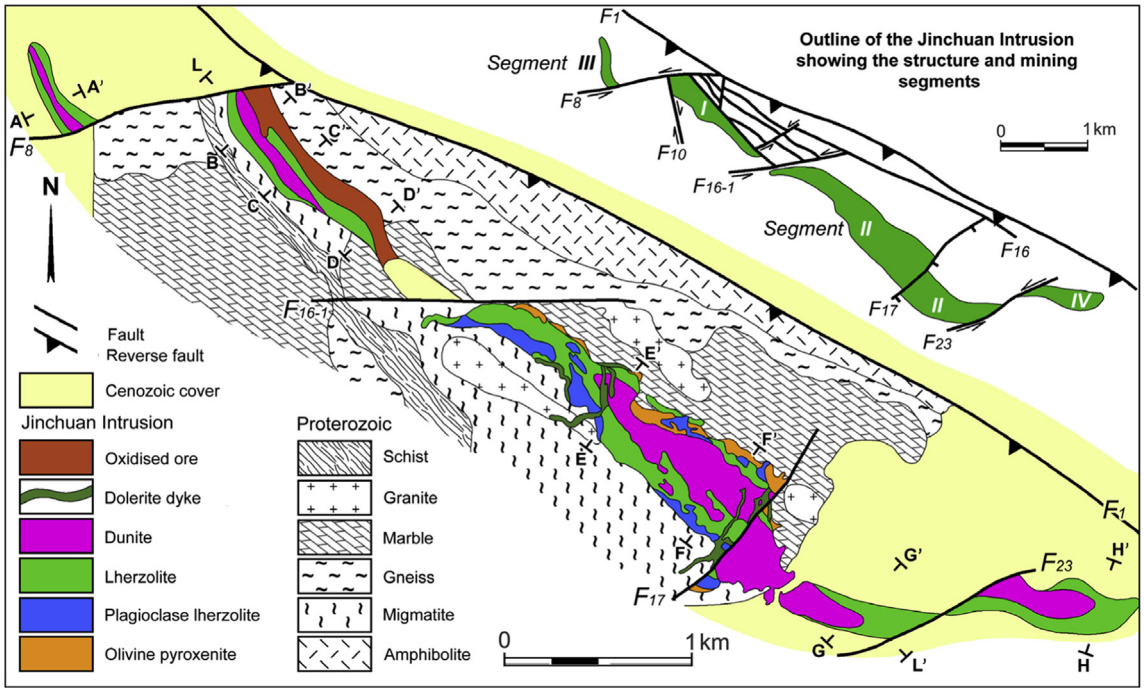

Figure 3. Geology and structure of the Jinchuan ultramafic intrusion and enclosing wall rocks. Top right inset shows the outline of the undifferentiated Jinchuan intrusion in green, the key faults and the four mining segments. The location of the longitudinal projection L–L′ in Fig. 4 and cross sections in Figs. 5 and 6 are also indicated (Geology after Song et al., 2012a,b).

a series of four mining segments from west to east, labelled III, I, II and IV (e.g., F_8 and $F_{16\text{-}1}$). Displacement on these faults, which may offset the NW–SE reverse fault set, is variable. They occur as 2 to 3 m wide breccia zones filled with Palaeoproterozoic and ultramafic intrusive rock clasts, and fault gouge;
- NNW–SSE striking dextral strike-slip faults, which may be cut by the preceding ENE–WSW set, but are rare at Jinchuan (e.g., F_{10});
- NE–SW striking normal faults (e.g., F_{17}).

4.6. Jinchuan ore deposit

The fault defined mining segments I, II, III and IV described above, have no petrological significance as the structures that separate them are all post-magmatic. Chai and Naldrett (1992) carried out systematic petrological and geochemical studies on the Jinchuan intrusive rocks, and divided the igneous complex into three magma sub-chambers, the West, West-central and East (Fig. 4). These sub-chambers did not initially include the fault-displaced segments III and IV at the extremities of the ore zone, but which are now known to comprise the lateral extensions of the West and East sub-chambers, respectively. Their West sub-chamber corresponds to segment I, while segment II is divided into the West-central and East sub-chambers.

Based on the geometry and the distribution of rock types within the intrusion, they divided the intrusion into two parts: a laterally zoned western part, including the West and West-central sub-chambers, and a vertically layered eastern part, that corresponds to the Eastern sub-chamber. Chai and Naldrett (1992) regarded the two sub-chambers of the western part of the intrusion as being characterised by a similar tabular shape and lateral zoning pattern, which include a dunite core, lherzolite wings and olivine pyroxenite margins. At the outer contact between the intrusive and country rocks, the intrusive rocks are often sheared, occurring as a 0 to 5 m thick chlorite-serpentine schist zone. Inboard from the contact, the olivine pyroxenite margins are usually <40 m thick and locally discontinuous, being slightly thicker on the northern side of the intrusion, although the reverse is observed locally.

The lherzolite predominates on the lateral wings of each sub-chamber, particularly in the up-dip parts/wings of the intrusion, where it reaches a width of nearly 300 m at the surface, but also occurs as a layer in the footwall and hanging wall of the dunite core. The dunite core is usually ~50 to 150 m thick, and extends for more than 500 m vertically. It has a lens-like shape, paralleling the walls of the intrusive body, and as indicated above, is enveloped by lherzolite on all sides in most locations. The deeper parts of the intrusion are almost entirely composed of sulphide-bearing dunite, with the lherzolite halo being absent or only occurring as a thin marginal rim in the footwall and hanging wall of the dunite. In the upper sections of the intrusion, local developments of plagioclase lherzolite are encountered, occurring as narrow, discontinuous bands that are usually <10 m thick. Towards the east, these zones become more numerous and coalesce to form a plagioclase lherzolite layer, which characterises the eastern part of the intrusion (Chai and Naldrett, 1992; Naldrett, 2004).

The eastern part of the intrusion, which Chai and Naldrett (1992) equated with East sub-chamber, is described by those authors as having a much broader, boat-like profile with a "V-shaped" cross section, and has markedly different characteristics. Although it has a very thin, <20 m rim of olivine pyroxenite, all of the other rock types have a shallow layering and are largely concentrated in the deeper parts of the intrusion. Dunite is predominantly located near the base of the intrusive body and is closely associated with the sulphide mineralisation. There is a rapid upward transition to lherzolite, then to plagioclase lherzolite and back to lherzolite again at the top. This interpretation of the Jinchuan ultramafic intrusion was generally accepted in the literature until ~2010, in which most authors (e.g., Chai and Naldrett, 1992; Tang, 1993; Ripley et al., 2003; Naldrett, 2004) regarded the different segments and sub-chambers of the Jinchuan intrusive complex as a single elongate intrusion, dismembered by late faults. However, ongoing drilling and underground development at the deposit provided new data, and allowed the understanding of the deposit to advance.

Song et al. (2012a,b) proposed that there are independent Eastern and Western intrusions, separated by fault $F_{16\text{-}1}$. The former corresponds to the East and West-central sub-chamber of segments II and IV, whilst the West sub-chamber, and mining segments I and III, represent the Western intrusion. The Western intrusion comprises two separate units, with regular planar variations in lithology and chemistry, interpreted as magmatic mega-cycles, whilst the Eastern intrusion is characterised by a concentric distribution of rock types with a core of sulphide-bearing dunite that is enveloped by lherzolite, consistent with the description of the West-central sub-chamber by Chai and Naldrett (1992).

4.6.1. Western intrusion

The section of the Western intrusion in mining segment I (Figs. 3 and 5), strikes NW–SE and dips to the SW, is 1500 m long, and extends to depths of >700 m beneath the surface. The thickness of the combined intrusion in this segment varies from ~300 m on its western extremity to <30 m in the east near fault $F_{16\text{-}1}$. Segment III,

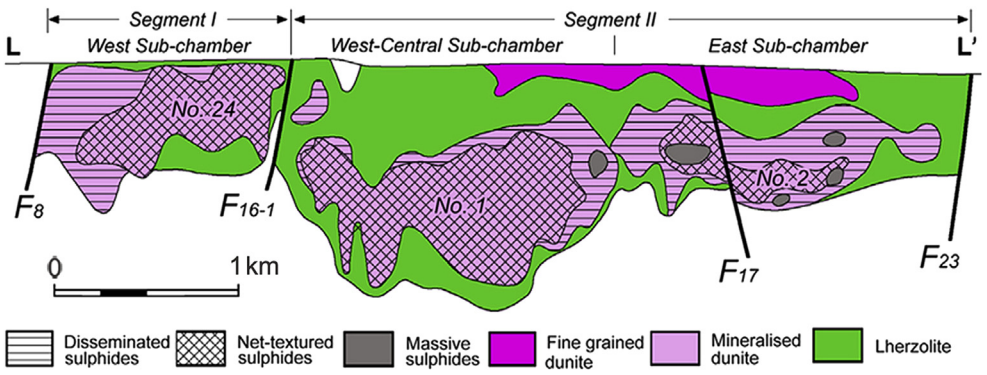

Figure 4. Longitudinal projection along the Jinchuan ultramafic intrusion segments I and II, showing ore types, ore deposits and intrusive lithologies (after Song et al., 2012a,b). See Fig. 3 for section location.

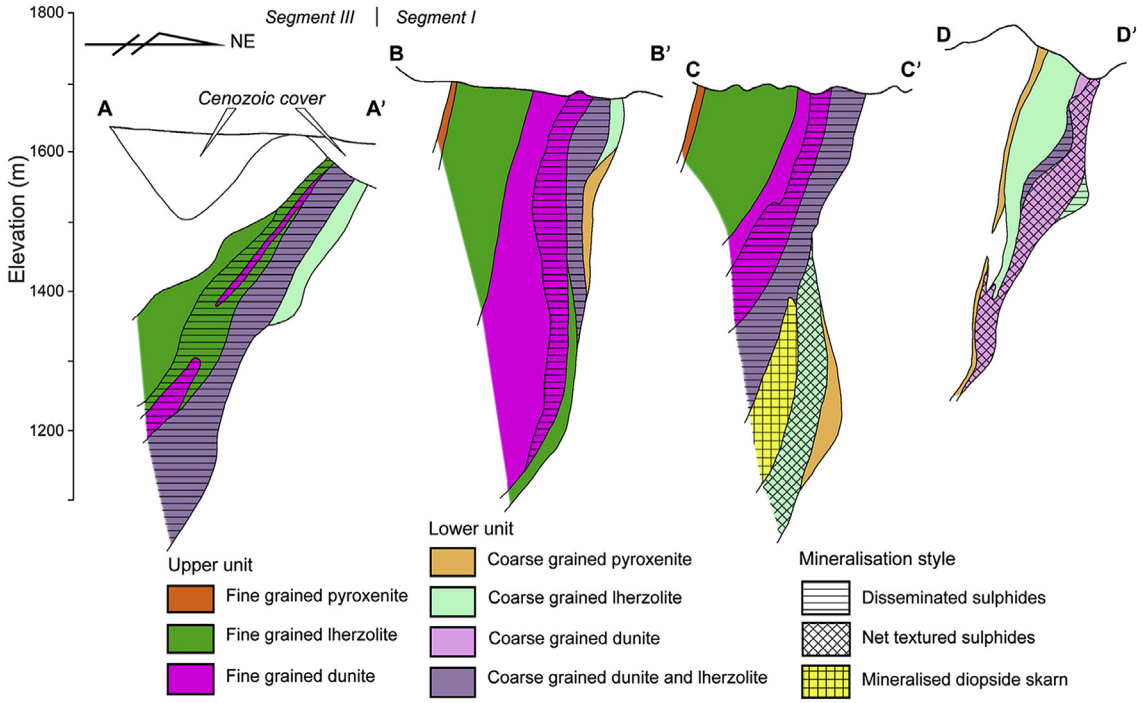

Figure 5. Representative cross sections showing the geology and mineralisation of the western Jinchuan ultramafic intrusion, in segments I and III (after Song et al., 2012a,b). See Fig. 3 for section locations. Note that the intrusion continues down dip to the southwest, well beyond the sections coloured on sections A–A′, B–B′ and C–C′.

which is north of fault F_8, is 500 m long with a thickness of 250 m at its eastern termination and extends for more than 600 m beneath the surface, dipping to the southwest (Song et al, 2012a,b).

The Western intrusion comprises two megacycle suites, the Lower and Upper units, which are separated by a sharp contact that roughly parallels the northern walls of the intrusion. The two units have different lithologic features, and although each exhibits an upward decrease in olivine content, are distinguishable on the basis of both rock types and textures (Song et al, 2012a,b). The Upper unit is largely devoid of sulphides, other than weak disseminations at its base, whilst disseminated, net-textured and minor massive sulphides in the Lower unit constitute the No. 24 Orebody (Chen et al., 2013).

4.6.1.1. Lower unit. The Lower unit, which occurs in both segments I and III, is mainly composed of coarse-grained olivine-sulphide cumulate dunites, overlain by coarse-grained lherzolite, with limited amounts of pyroxenite at the base. The olivine grains of the coarse-grained dunites and lherzolites vary from 4 to 7 mm in size, and occasionally up to 10 mm, and are either in contact, or isolated from each other by sulphides, or included in large oikocrysts of clinopyroxene. Sulphides are concentrated in the lower sections of the Lower unit in both segments I and III (S.G.U., 1984; Song et al, 2012a,b).

In segment I, the Lower unit dunites and lherzolites contain 5 to 25% sulphides, and constitute the northwest striking, 1500 m long, southwest dipping, *No. 24 Orebody*, the third largest at Jinchuan. This orebody is generally 20 to 70 m thick, but may be as much as 130 m where the Lower unit thickens. The sulphides within this orebody occur within dunite and lherzolite, towards the footwall of the chamber. Disseminated and net-textured ores (1 to 4 wt.% Ni), account for >95% of the sulphides. Disseminated ore dominates in the western part of the orebody, thickening westward, to a width of >200 m at its widest, and extending into segment III, but thinning eastward and down dip, with local bifurcation (S.G.U., 1984; Song et al, 2012a,b). The disseminated ores generally have a modal composition of 3 to 15% sulphides, comprising 1 to 8% pyrrhotite, 1 to 5% pentlandite, and 1 to 3% chalcopyrite, as well as 0.1 to 1.2% magmatic magnetite, which are either enclosed in silicate crystals or are interstitial between them (S.G.U., 1984; Chen et al., 2013).

Net-textured ore is absent in the west of segment I and in segment III. It appears as a small lens close to the footwall of the orebody, widening eastwards (up to 60 m) and with depth. In the east, the net-textured ore is enveloped by disseminated sulphides, which are usually thicker on the hanging wall side. The modal composition of the net-textured ores comprises 15 to 40% sulphides, including 10 to 30% pyrrhotite, 4 to 10% pentlandite and 1 to 4% chalcopyrite (S.G.U., 1984; Naldrett, 2004).

More than 12 PGE enriched lenses have been defined within the No. 24 Orebody, distributed in the net-textured ore, parallel to the Ni-Cu sulphide orebody, with occasional irregularities along fracture zones. These fracture zones can be very enriched in PGE, e.g., one with a strike length of >100 m and width of 1 to 1.4 m, with an average grade of 6.15 g/t Pt and 1.83 g/t Pd (S.G.U., 1984; Naldrett, 2004).

Small massive sulphide bodies occasionally occur in the eastern parts of the No. 24 Orebody, within the net-textured ores, with a modal composition of 50 to 70% pyrrhotite, 10 to 20% pentlandite and minor (1 to 7%) chalcopyrite. Anhedral pentlandite crystals occur between anhedral or subhedral pyrrhotite grains or as exsolution flames in pyrrhotite. Both the net-textured and massive sulphides contain significant magmatic magnetite contents, varying from 1.01 to 4.4% (S.G.U., 1984).

Marble xenoliths, which are found in both segments, have been altered to form a diopside skarn interlayer (Fig. 5), consisting of 70 to 85% diopside, 15 to 25% calcite, minor titanite and iddingsite, with pseudomorphs of olivine, and variable amounts of sulphides (up to 10%). The abundance of olivine in the coarse-grained dunite zone gradually decreases upward from the skarn interlayer, from

~90 to ~70%, while the underlying lherzolites contain 50 to 60% (Song et al, 2012a,b).

Copper-rich sulphide pods occur at the base of the No. 24 Orebody (S.G.U., 1984) as described above (*Ore Styles and Textures* Section 4.3).

4.6.1.2. Upper unit. From the base to the top, the Upper unit of the Western intrusion is composed of fine-grained dunite, lherzolite and minor pyroxenite, reflecting the decreases in olivine and gradual upward increases in pyroxene, although 0.5 to 3 mm olivine crystals are enclosed in large oikocrysts of clinopyroxene in these rocks. The Upper unit is generally sulphide poor, although the dunite at the base of the unit in segment I contains up to 5% interstitial sulphides. The sulphides are interstitial between olivine and pyroxene grains and are composed of pyrrhotite, pentlandite and minor chalcopyrite. In segment III, lherzolite may also contain sulphides where the dunite becomes very thick (Naldrett, 2004; Song et al, 2012a,b; Chen et al., 2013).

The MgO content within the Upper unit decreases upward, from 42 to 45 wt.% in the dunites, to 36 to 41 wt.% in the lherzolites, while Al_2O_3 and incompatible elements increase upward. In contrast, the MgO content of the Lower unit progresses from a 37 to 40 wt.% range in the coarse-grained dunites, to 28 to 35 wt.% in the overlying lherzolites. These geochemical trends, combined with the sharp contact between the units, and the presence of fine-grained dunite xenoliths at the top of the Lower unit, suggest the Lower unit is younger, and was intruded along the base of the Upper unit (Song et al, 2012a,b).

4.6.2. Eastern intrusion

The Eastern Intrusion is dominantly composed of medium- to coarse-grained lherzolite and sulphide-bearing dunite, with fine-grained dunite only occurring at the top of mining segment II. The intrusion in segment II, contains a core of net-textured sulphide-bearing dunite, with a thin margin of disseminated sulphide-bearing dunite, which in turn, is enveloped by coarse-grained lherzolite. The sulphide-bearing dunite in the West-central sub-chamber of this segment constitutes the *No. 1 Orebody* (Figs. 4 and 6), which is lens-shaped, 1500 m long, up to 120 m thick, and extends from 200 to >1100 m below the surface. This orebody contains ~50% of the Ni, Cu, and PGE resources of the Jinchuan deposit (Song et al, 2012a,b). Mineralisation is dominated by net-textured sulphide ore, enveloped by low-grade disseminated ore at both ends and in the upper part of the orebody. The ore has very high PGE and Au concentrations, with the best PGE enrichment in a 500 m long and up to 47 m thick lens in the lower part of the orebody, which is sub-parallel to the margins of the Ni-Cu orebody. This lens averages 2.4 g/t Pt, but locally is as high as 9 g/t. Several other smaller and lower grade PGE enriched sections are also known (Naldrett, 2004).

The *No. 2 Orebody*, which is ~1300 m long and up to 118 m thick, occurs near the base of the East sub-chamber, in the eastern section of mining segment II (Figs. 4 and 6), and is composed of sulphide-bearing dunites in the lower part of the intrusion, overlain by medium to coarse-grained lherzolite (S.G.U., 1984; Chai and Naldrett, 1992; de Waal et al., 2004; Li et al., 2004; Song et al., 2009b). It includes a >900 m long by 40 m wide body of net-textured ore below a zone of disseminated mineralisation. Eastward, the net-textured ore gradually decreases in width and disseminated ore becomes dominant, accounting for ~59% of the nickel reserve of the orebody. This is one of the small number of locations at Jinchuan containing massive ore (4 to 9 wt.% Ni), as described in the *Ore Styles and Textures* Section 4.3.4. above.

The continuation of the same mineralised zone in mining segment IV is 1300 m long, up to 230 m wide, and dips at 50° to 60°SW (Fig. 6). The geology and mineralisation are comparable to No. 2 Orebody in the eastern part of segment II, containing disseminated sulphides, overlain by medium- to coarse-grained lherzolite. The western margin of segment IV has been extensively deformed by fault F_{23}, which separates it from segment II (Song et al, 2012a,b).

Chen et al. (2013) showed that the Eastern intrusion has similar Ni and Cu tenors to those of the Western intrusion. However, compared to the Eastern intrusion, the sulphides of the Western intrusion contain slightly higher whole-rock PGE contents at the same S concentrations, and the disseminated sulphides of the Nos. 1 and 2 orebodies in the Eastern intrusion have markedly lower PGE tenors than those of the No. 24 orebody, as well as higher Cu:Pd ratios (10,000 to 548,000, mostly >30,000; Song et al., 2009b). The net-textured and massive sulphides of the Nos. 1 and 2 orebodies show similar Pt depletion to those of the No. 24 orebody, but have much larger variations in Iridium group PGE than

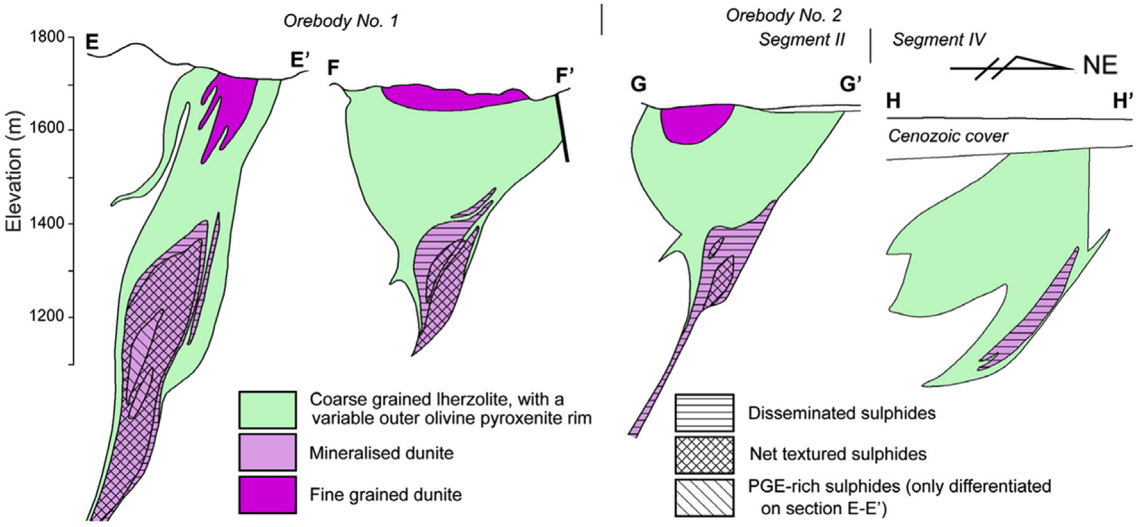

Figure 6. Representative cross sections showing the geology and mineralisation of the eastern Jinchuan ultramafic intrusion, in segments II and IV (sections E–E′ and G–G′ after Song et al., 2006; sections F–F′ and H–H′ after Song et al., 2012a,b). See Fig. 3 for section locations.

those of the No. 24 orebody. Chen et al. (2013) interpreted these geochemical contrasts and the differences in spatial distribution of the types of sulphide mineralisation between the two intrusions, to suggest they segregated from distinctly different parental magmas and experienced different fractionation processes.

The MgO content of the western portion of the Eastern intrusion varies from a range of 38 to 45 wt.% in the sulphide-dunite core, to <25 wt.% in the marginal lherzolites, coupled with increases in TiO_2, Al_2O_3, CaO, and incompatible trace elements (Song et al, 2012a,b).

4.7. Post-magmatic alteration

Much of the Jinchuan ultramafic intrusion has been overprinted by low-grade metamorphism, hydrothermal alteration and near-surface oxidation, as recognised by Chai and Naldrett (1992), Barnes and Tang (1999), de Waal et al. (2004), Li et al. (2004), Ripley et al. (2005) and Lehmann et al. (2007), with magmatic minerals being variably preserved throughout the intrusion. In some places alteration is negligible, in others, all primary phases have been transformed into an assemblage of serpentine, tremolite-actinolite, chlorite and magnetite (Tang and Li, 1995a,b; Lehmann et al., 2007). Olivine within the intrusion has been found in various states of replacement by serpentine, chlorite, amphibole and fine-grained magnetite, whilst the interstitial pyroxene and minor plagioclase have been locally converted to chlorite, amphibole, epidote, clinozoisite and more Na-rich feldspar, with lesser amounts of calcite. In addition, up to 30 (averaging 10) vol.% of the sulphide minerals have been replaced by magnetite, serpentine and chlorite. The preserved interstitial net texture of sulphide minerals surrounding altered olivine grains, which remain undeformed, suggests replacement of sulphides by secondary magnetite and silicates was isovolumetric (Ripley et al., 2005).

de Waal et al. (2004) proposed two main alteration stages to explain these assemblages. In the first, interstitial orthopyroxene, clinopyroxene and plagioclase were altered to fine-grained amphibole (tschermakite, actinolite-tremolite), garnet (andradite), chlorite and talc. In the second, lower-temperature stage, olivine was extensively replaced by serpentine ± magnetite, whereas the chromian spinel was commonly altered to an aluminous spinel. In the early stage of alteration, prior to the loss of sulphur, pentlandite is altered to millerite and magnetite, pyrrhotite to pyrite, and chalcopyrite is converted to violarite or cubanite (Prichard et al., 2013).

Li et al. (2004) observed the progression of this alteration in samples where incipient modification of interstitial pyroxene has produced Mg-hornblende and chlorite, and the rims of coexisting olivine are recrystallised to form a more Fe-rich variant. With the progress of alteration, tremolite replaces the Mg-hornblende, and the size of the recrystallised Fe-rich olivine rim increases. These processes involve the release of Mg from forsterite-rich olivine. At the most advanced stage of this alteration, a characteristic mosaic texture is developed, caused by the intergrowth of randomly oriented actinolite needles with completely recrystallised, Fe-rich olivine (fayalite). The recrystallised olivine in these samples (which has not proceeded to the serpentinisation stage) contains forsterite and Ni that are respectively up to 8 mol.% and 500 ppm lower than primary olivine. In contrast, the subsequent serpentinisation of olivine had a less marked influence, with the forsterite and Ni contents of remnant olivine kernels and unaltered crystals from the same sample overlapping the serpentinised olivine. This subsequent, lower temperature serpentinisation of olivine and sulphide minerals at Jinchuan results in a loss of metals and sulphur from the sulphide minerals. The process is largely controlled by micro-fractures, as seen in the development of serpentine ± chlorite and magnetite mesh textures of fine ribbons and veinlets in olivine and the occurrence of magnetite, serpentine and chlorite veins in sulphide minerals. Ripley et al. (2005) interpreted this veining to reflect a near-isovolumetric replacement process, driven by fluid infiltration and solution and redeposition on a centimetre scale along microfractures. The serpentinisation [$Mg_{2.75}Fe_{0.25}Si_2O_5(OH)_4$] of sulphides requires the local addition of Mg and Si from hydrolysis of olivine, pyroxene and plagioclase (Ripley et al., 2005). Pyrite, which is found in these late-stage calcite-pyrite-serpentine-magnetite veins and veinlets, has negative $\delta^{34}S$ values, consistent with a partial reduction of sulphate produced during fluid-induced oxidation of the primary sulphides and reprecipitation in late pyrite veins (Ripley et al., 2005). However, while some of the metals and sulphur lost in the serpentinisation process have been taken up in vein redeposition, this has been estimated to account for <1% of the metals lost during replacement of the sulphides (Ripley et al., 2005).

Ripley et al. (2005) conducted oxygen and hydrogen isotope studies of silicate minerals at Jinchuan that suggest a complex history of hydrothermal alteration, involving rock interaction with at least two distinct fluids (high and low δD). They found that the compositions of oxygen and hydrogen isotopes in amphibole, and oxygen isotope compositions of feldspar and serpentine, are all consistent with the involvement of evolved meteoric water or seawater. They noted that, while the involvement of metamorphic fluids cannot be excluded, the H_2O deficient nature of the pre-intrusion metamorphic rocks, and the high water/rock ratio required for the alteration, as indicated by isotopic relationships, are more consistent with the participation of a large fluid reservoir. They also note that the actual range of serpentine δD values may be explained by a number of different reactions with meteoric water and either a metamorphic water or seawater. However, whatever the reaction, they conclude the large volume of fluid that appears to have interacted with ultramafic rocks at Jinchuan, is consistent with large-scale hydrothermal convection and an extension/rift-related origin for the magmatism. This is taken to suggest that the intrusion was emplaced in an extensional regime, below a developing rift basin. The rift basin is reflected by the Neoproterozoic Denzigou Formation sequence, which is exposed within a few kilometres of the deposit. Reflux of large volumes of oxidised and acidic meteoric brines, and/or seawater, is interpreted to have been drawn down from a reservoir in the coarse rift-sag sequence. This fluid may have been circulated via the extensional fault framework, to interact with the hot mineralised intrusion, which, in turn, drove the convection cell (e.g., Prichard et al., 2013).

Based on the mineral assemblages present in the alteration products, Ripley et al. (2005) estimated the alteration sequence to have been due to two pulses, or a single progressively cooling fluid, at temperatures between ~400 and 275 °C. Prichard et al. (2013) suggested the alteration has also affected the distribution and form of platinum group element (PGE) occurrence. The altered rocks from the Jinchuan intrusion host far more platinum group minerals (PGM), especially Pd-bearing PGM, compared to the fresher samples where PGE are found within the base metal sulphides. It is interpreted that Pd, which first partitioned into pentlandite during magmatic crystallisation, has exsolved from the base metal sulphides during post-magmatic alteration, and subsequently re-crystallised in PGM, particularly as froodite [$PdBi_2$] phases. Further speculations indicate that the first, higher temperature stage of alteration that affected the interstitial silicates, also led to partial transformation of some of the base metal sulphides into magnetite, and the release of some PGE from the base metal sulphides to form PGM in association with silicate alteration minerals. The second alteration phase, associated with the serpentinisation of the base metal sulphides, with locally up to 30%

being converted to magnetite, released further contained PGE, which were re-deposited as PGM associated with the alteration magnetite. The range of PGM and their distribution relative to sulphide, magnetite and silicate mineral assemblages are given in Section 4.2 *Ore Mineralogy*. These alteration processes have substantially affected the bulk geochemistry of the intrusion and its metal content.

5. Discussion

The intrusion that hosts the Jinchuan Ni-Cu-PGE deposit, is one of a large number (>100) of northwest elongated, ultramafic intrusive bodies within a >100 km long, northwest trending corridor, exposed within the similarly trending Cenozoic Longshoushan Terrane uplift (Song et al, 2012a,b). These intrusions, which include both barren and lesser sulphide-mineralised bodies, were emplaced at ~827 Ma (Li et al., 2005), during an extensional event that presaged the breakup of the Rodinia supercontinent, which was not completed until more than 100 to 200 Myr later (Li et al., 2008).

The deposit is < 25 km northeast of the current southwestern margin of the North China Craton. The craton margin is defined by its boundary with the northwest trending allochthonous rocks of the Palaeozoic Qilian Orogen. These younger rocks are estimated to have been thrust ~300 km to the northeast, over the craton, during the Cenozoic (Champagnac et al., 2010). This means, the Jinchuan deposit was most likely emplaced several hundred kilometres to the northeast of the Rodinia break-up margin of the North China Craton. However, it was possibly intruded below an intracontinental rift basin into which the overlying Neoproterozoic Denzigou Formation rift-sag sequence rocks were deposited. The Denzigou Formation rocks do not directly overlie the mineralised intrusion, but are exposed within a few kilometres of the deposit (Prichard et al., 2013).

Chai and Naldrett (1992) and de Waal et al. (2004) calculated that the parental magma of the Jinchuan intrusion was most likely a high-MgO to picritic basalt, containing 11.5 wt.% MgO, 11.2 wt.% FeO and 330 ppm Ni, whilst Chen et al. (2009) and Li and Ripley (2011) later estimated that it had 12.3 to 12.6 wt.% MgO.

Li et al. (2005) suggested that the integrated mineralogical, petrological and geochemical data are consistent with the generation of the parental magma of the Jinchuan ultramafic intrusion through high degree melting of long-term enriched sub-crustal lithospheric mantle (SCLM) by an anomalously hot mantle plume with a potential temperature (T_p) of >1350 °C. Other authors support this conclusion (e.g., Barnes and Lightfoot, 2005; Ripley et al., 2005; Lehmann et al., 2007; Begg et al., 2010; Song et al., 2012c). This plume is taken to be part of the global event that initiated the break-up of Rodinia (e.g., Li et al., 2008).

When a substantial mass of hot SCLM melt is produced, it will buoyantly rise through the denser, colder SCLM, ahead of the plume head, towards the Moho, which acts as a gravity barrier. As the lighter melt rises, it produces lateral visco-elastic magmatic channel spreading in the upper SCLM. This channel spreading prompts extension at the base of the crust, which triggers upwards propagating, conjugate normal faulting into the crust, and subsidence in graben-like depressions at the surface, as indicated in detailed modelling of this type of system by Gerya and Burg (2007). If the ductile lower crust is relatively weak, or of low density, the SCLM melt will pool along the Moho and form a mafic underplate rather than rise into the less dense crust.

However, it is likely that the lower crustal transition in this part of the North China Craton is occupied by a dense, strong layer associated with crustal attenuation and mafic underplating responsible for the high-temperature metamorphism and migmatisation of the Palaeoproterozoic Baijiazuizi Formation and the late Palaeoproterozoic rifting represented, in part, by the overlying Tamazigou Formation.

Where the lower crust is relatively dense and sufficiently strong, a large mass of hot SCLM melt can cross the Moho and follow the major normal fault system it has generated, buoyed by the hydraulic upthrust produced by the density contrast from the underlying melt chamber in the SCLM. Upward propagation into less dense crust will continue until the mass of the intruding column balances the upthrust exerted from below the Moho, or the intrusion can follow a lateral path within the less dense crustal rocks. When a lateral weakness is encountered, e.g., a stratigraphic/lithologic contrast, or a shallow dipping structure such as an extension related listric fault/décollement, the intrusion will mushroom to form a horizontal magma chamber rather than continue rising against gravity into less dense crustal rocks.

de Waal et al. (2004), Li et al. (2004), Song et al. (2006, 2009a,b, 2012a,b), Prichard et al. (2013) concluded that the parental magma of the Jinchuan intrusion was initially entrapped in a very large staging chamber, or series of sub-chambers, where it underwent fractional crystallisation, prior to expulsion. Initial crystallisation within this large staging chamber is supported by calculations by Chai and Naldrett (1992) and Li et al. (2004) that the volume of magma in the Jinchuan intrusion accounts for <2% of the total parental magma required to generate the amount of olivine in that intrusion. Secondly, the same authors show that it also represents only ~3% of the total magma required for the sulphides within the same intrusion, i.e., ~97% of the magma required to produce the Jinchuan deposit is not contained within the Jinchuan ultramafic intrusion.

Before entering the staging chamber, the S-undersaturated and PGE-undepleted high-MgO basaltic magma is interpreted to have undergone crustal contamination, which promoted incipient crystallisation of minor (<5 wt.%) olivine, orthopyroxene (as inclusions in the cumulus olivine) and chromian spinel (as inclusions in the cumulus orthopyroxene). This took place during ascent from the Moho, either *en route*, or in another intermediate staging chamber, at depths of >9 km (where $P = 2.8$ kbar; de Waal et al., 2004; Song et al., 2009b). If the sulphur was contained within the magma from below the Moho (see the *Sulphur* Section 4.4 above), and not ingested from the crust during ascent, the sulphur solubility must have been extensively lowered by means of input of a large amount of SiO_2 and Al_2O_3 contamination (Song et al., 2011). During this period, as sulphur was saturated, a small quantity of sulphides (~0.008 wt.%) formed, scavenging PGE and leaving the basaltic magma significantly PGE-depleted (Song et al., 2009b).

According to de Waal et al. (2004), Li et al. (2004) and Song et al. (2006), after the now contaminated, S-saturated and PGE-depleted basaltic magmas reached the staging chamber, orthopyroxene was replaced on the liquidus by olivine, which then began crystallising, whilst at the same time, sulphide droplets commenced to exsolve from the magma. Both olivine crystals and sulphide droplets settled to the bottom of the chamber under the influence of gravity. Olivine replaces orthopyroxene as the liquidus mineral at P between 2.8 and 1.3 kbar, which implies the staging chamber was at a depth somewhere between ~9 and ~4 km below the surface.

The relatively more fluid and denser sulphide droplets, coalesced, sank, and began to displace the interstitial silicate magma of the olivine cumulates at the base of the staging chamber to form a bottom layer of pure sulphide. Such a crystal-liquid differentiation process produced a stratified sulphide-olivine-magma column. Once olivine crystals became engulfed in the heavier sulphide liquid, crystal overgrowth ceased, resulting in variable grain-sizes and similar forsterite compositions of olivine in the

sulphide-rich layer close to the bottom of the chamber (de Waal et al., 2004).

A crystal-mush layer of jostled olivine, orthopyroxene and chromian spinel crystals, formed above the sulphide-rich layer. These are, in turn, overlain by an upper, relatively crystal-free residue (de Waal et al., 2004; Song et al., 2009b).

As the buoyant mantle plume below continued to rise and melt more SCLM, further intermediate density, un-segregated magma was supplied to the staging chamber, entering at the density transition between the base of the lighter, upper crystal free residue band, and the denser underlying crystal mush and sulphide layers (de Waal et al., 2004; Song et al., 2009b).

New pulses of magma entering the staging chamber may have different contamination and segregation histories. Sulphides that crystallised from these later pulses only settled part way down through the olivine crystal mushes formed earlier, or started a new stratification with different characteristics (Song et al., 2009b).

The hydraulic pressure of incoming new magma, driven by the density contrast buoyancy below the Moho, produced one or more of three potential outcomes, namely (i) further lateral expansion of the staging chamber, (ii) 'pumping up' of the chamber to cause updoming when the hydraulic pressure exceeds the lithostatic pressure, or (iii) expulsion of sections of the contents of the chamber along available or newly created fractures.

Sections of the upper crystal-free residue in the staging chamber, with relatively low yield strength and viscosity, were the first to be squeezed out, to form the sulphide-barren mafic intrusions in the Jinchuan area (e.g., Xijing, Maocaoquan and Dongwan; Fig. 2). Subsequently, the high yield-strength, relatively viscous, high-density olivine- and sulphide-laden mushes at the base of the staging chamber were injected into nearby planar fractures/faults to form the Jinchuan intrusion, at a depth estimated to be >4 km, on the basis of phase relationships of cumulus olivine and orthopyroxene in the rocks.

Chai and Naldrett (1992) and Tang (1993), regarded the Jinchuan ultramafic intrusion to be a dyke. Chai and Naldrett (1992) further proposed that the intrusion represents the fault controlled root zone of a much larger layered intrusion that has since been eroded. However, de Waal et al. (2004) and subsequent authors, have interpreted it to have originally been a relatively flat sill-like body. This interpretation is based on the observation, that, irrespective of the current dip of the deposit, which varies along strike from <20° to near 70°, the sulphide zones are not confined to the deepest part of the deposit, but tend to be found close to the northern side wall (or footwall). They suggest the northern side wall was the base of the sill, and that since emplacement, the planar deposit has been rotated to its present attitude, and dislocated into 4 segments by faulting, during Palaeozoic and/or Cenozoic deformation. de Waal et al. (2004) suggested the deposit was emplaced as a semi-conformable body, controlled by pinches and swells in a sub-horizontal planar fault developed at the competency contrast between marbles and overlying gneisses.

Mapping shows that, although the southern (originally upper) contact with felsic gneisses is sheared, the northern (lower) contact appears to be intrusive. On a broad scale, the intrusion is conformable with the foliation of the surrounding rocks, but is locally discordant, and strikes obliquely to relict bedding in the marbles (Lehmann et al., 2007).

Song et al. (2012a,b) have suggested the deposit was originally two separate, but close, Western and Eastern sill-like intrusions with different characteristics, and that the former was at a lower stratigraphic position, each having been dislocated into two segments and juxtaposed by subsequent sinistral strike-slip faulting. Song et al. (2012a,b) also suggested the fault dislocation into segments occurred primarily during the Cenozoic and is a response to movement on the major F_1 fault that forms the northern margin of the Longshoushan Terrane uplift. Song et al. (2012a,b) noted the difference in character between the Eastern and Western intrusions, and between the Upper and Lower units of the latter, and suggested contributions from injections of sulphide-free and sulphide-bearing olivine-crystal mushes from three separate staging chambers, each with a different magmatic history. Alternatively, the different magmas may be related to temporally separated expulsion pulses from the same, dynamically evolving staging chamber.

de Waal et al. (2004) proposed that the olivine- and sulphide-laden mushes, from the bottom of the staging chamber, were injected into the Eastern intrusion structure, and that the West-central sub-chamber represented the proximal part of the conduit through which the mushes entered. Olivine crystals and sulphide liquid became further concentrated in the centre of the conduit in response to a higher velocity in this regime to form the No. 1 Orebody. As the main mass of mushes moved into the conduit, flow differentiation resulted in light silicate liquid being more concentrated toward the outer walls to form a lubricant sheath to the viscous, high-strength intrusive core. In contrast, the eastern part of the intrusion, the East sub-chamber, is interpreted to represent a more distal front of the intruding mushes, with more chaotic fluid dynamics, resulting in more complex mingling of batches of mush and flow banding in these regimes where the No. 2 Orebody formed. In both sub-chambers, continued gravity settling meant that the sulphides concentrated towards the base of the sill (de Waal et al., 2004).

In the Western intrusion, Song et al. (2012a,b) postulated an initial input of magma from residue in the upper portion of a staging chamber that contained a segregated mass of originally PGE un-depleted magma. A number of pulses of fine-grained, relatively crystal free magma, containing minor olivine and sulphides, was ejected from the staging chamber, and injected into what became the West sub-chamber, to form the Upper unit. The small quantities of sulphides entrained in the magma of each pulse progressively settled to the base of the Upper unit to form a zone of low-grade disseminated mineralisation. Following emplacement of the Upper unit, sulphide- and olivine-bearing mushes from the base of a staging chamber entered the Western intrusion, along the basal contact of the cooled Upper unit, to form the Lower unit. The sulphides and olivine entrained in the magma settled, to form the No. 24 Orebody, whilst the overlying sulphide-poor residue in the upper part of the chamber was displaced by new surges of replenishing magma. The high Cu:Pd ratios of this orebody suggest, that, unlike the Upper unit, but like the Eastern intrusion, PGE-depleted magma was segregated in the source staging chamber of this magma (Song et al., 2012a,b).

As detailed above, the Jinchuan ultramafic intrusion, most likely comprises <3% of the total magma volume responsible for the sulphides contained within the deposit. Some of the balance flowed through the Jinchuan intrusion conduit to be deposited as intrusions elsewhere. No voluminous mafic volcanic sequences are recorded in the overlying Neoproterozoic Denzigou Formation rift sequence outcropping a few kilometres distant. It is likely that the bulk of this magmatic episode is concealed at depth in the major staging chamber, being too heavy to rise further through the much less dense crust, whilst much of the rest is in the large number of mafic to ultramafic intrusions in the district.

As the Jinchuan ultramafic intrusion cooled, it acted as a heat engine that promoted the circulation of meteoric and magmatic fluids towards the surface, which, in turn, resulted in the drawdown of cooler meteoric fluids from closer to the surface, through extensional faults, most likely from a large reservoir in the overlying rift sequence of the Denzigou Formation. This fluid circulation

led to the large-scale post-magmatic hydrothermal alteration of the ore deposit, as described above.

Following the break-up and dispersal of Rodinia during the late Neoproterozoic, accretion re-commenced with the Qilian and Qaidam blocks colliding with, and overriding the North China Craton to the southwest during the lower Palaeozoic. This collision was accompanied by voluminous granitic intrusion that extended as far north as the Jinchuan deposit. At the same time, subduction was active along the northern margin of the craton accreting new crust that was later amalgamated into the Central Asian Orogenic Belt.

During the late Palaeozoic to early Mesozoic, the North China Craton was sandwiched between the Central Asian and Central China Orogenic Belts, as the Siberian and Yangtze cratons advanced from the north and south respectively. Subsequently the Tethyan Belt developed as the Indian Craton approached from the south. Shortening related to the latter compressive event continues to the present day, with younger rocks from the south, advancing northeastward over the craton, above a northwest trending package of thrusts at the base of the Qilian Orogen succession.

6. Conclusions

The ~0.83 Ga Jinchuan ultramafic intrusion was emplaced during initiation of the Rodinia supercontinent break-up. It was intruded as a sill-like body into Palaeoproterozoic high temperature metamorphic wall rocks. The intruded rocks were basement to a northwest-southeast trending extensional rift basin within the Yinshan Block of the North China Craton. This intracratonic rift basin was >200 km from both the existing craton margin to the north and the subsequent break-up related margin to the south.

The parental magma of the Jinchuan intrusion was most likely a high-MgO to picritic basalt, generated through high degree melting of long-term enriched SCLM by an anomalously hot mantle plume. The density contrast of the hot SCLM melt caused it to buoyantly rise to the Moho.

The lower crustal transition in this part of the North China Craton is interpreted to have been occupied by a mafic underplate formed during late Palaeoproterozoic rifting. This transition appears to have been sufficiently strong and dense to allow the SCLM melt to cross the gravity barrier of the Moho into lighter crustal rocks, buoyed by the density contrast of a sufficiently large mass of that melt below the base of the crust.

The parental magma rose through the lower crust to a point where the mass of the intrusive column balanced the hydraulic upthrust from below the Moho and/or it encountered a shallowly dipping structural or lithological discontinuity that allowed it to pond into a large staging magma chamber at a depth of between ~9 and ~4 km below the surface.

During its passage through the crust, the melt was contaminated with significant amounts of SiO_2 and Al_2O_3, lowering the sulphur solubility. Cooling, crystallisation and settling of the resultant sulphur saturated magma within the staging chamber led to the development of a basal sulphide-rich band, overlain by a crystal-mush layer of jostled olivine, orthopyroxene and chromian spinel crystals, capped by a thicker, relatively crystal-free residue.

Continued input of new magma from below the Moho increased the hydraulic pressure within the staging chamber, resulting in expulsion of magma from different fractions in the settling column. These fractions were expelled along available or newly created fractures. Pulses of the sulphide and crystal mush layers were injected through a pair of *en echelon* structures to form the sill-like Jinchuan ultramafic intrusion. This intrusion, and the Jinchuan deposit, formed at a depth of >4 km by cumulus settling as expelled sulphide-rich magma passed through the structure. The resultant intrusion contains disseminated and net-textured sulphides in sulphide-dunite cores within a larger lherzolite sill complex. Temporally separated pulses tapped the staging chamber at different phases of its evolution, resulting in variations in character and composition across the Jinchuan intrusion and ore deposits. Magma expelled from the upper sections of the staging chamber produced the large number of barren to weakly mineralised intrusions in the surrounding district.

Following emplacement of the intrusion, reflux of large volumes of water, possibly from a reservoir in the overlying intracratonic rift basin, resulted in extensive post-magmatic alteration of both the intrusion and mineralisation.

Lower Palaeozoic orogenesis to the south produced voluminous granitoid intrusions that extended northward to the ore deposits. During the Cenozoic, Himalayan compression transported a northeast-vergent allochthonous sheet of Palaeozoic rocks ~300 km over the craton to within 25 km of the Jinchuan deposit. In a further response to this Cenozoic shortening, the Longshoushan Uplift, an elongate, downward tapering faulted wedge, was uplifted by > 4 km to expose the Jinchuan deposit in a window penetrating younger cover rocks. During this same event the intrusion was tilted and fragmented into four structural segments.

References

Barnes, S.-J., Lightfoot, P.C., 2005. Formation of magmatic nickel sulfide deposits and processes affecting their copper and platinum group element contents. In: Hedenquist, J.W., Thompson, J.F.H., Goldfarb, R.J., Richards, J.P. (Eds.), Economic Geology, 100th Anniversary Volume. SEG, Denver, pp. 179–214.

Barnes, S.J., Tang, Z., 1999. Chrome spinel from the Jinchuan Ni-Cu sulfide deposit, Gansu Province, People's Republic of China. Economic Geology 94, 343–356.

Begg, G.C., Hronsky, J.A.M., Arndt, N.T., Griffin, W.L., O'Reilly, S.Y., Hayward, N., 2010. Lithospheric, Cratonic, and Geodynamic Setting of Ni-Cu-PGE Sulfide Deposits. Economic Geology 105, 1057–1070.

Le Bas, M.J., Keller, J., Tao, K., Wall, F., Williams, C.T., Zhang, P.-S., 1992. Carbonatite dykes at Bayan Obo, Inner Mongolia, China. Mineralogy and Petrology 46, 195–228.

Chai, G., Naldrett, A.J., 1992. Characteristics of Ni-Cu-PGE mineralization and genesis of the Jinchuan Deposit, Northwest China. Economic Geology 87, 1475–1495.

Champagnac, J.D., Yuan, D.-Y., Ge, W.-P., Molnar, P., Zheng, W.-J., 2010. Slip rate at the north-eastern front of the Qilian Shan, China. Terra Nova 22, 180–187.

Chen, W.P., Chen, C.Y., Nabelek, J.L., 1999. Present-day deformation of the Qaidam Basin with implications for intra-continental tectonics. Tectonophysics 305 (1–3), 165–181.

Chen, L.M., Song, X.Y., Danyushevsky, L.V.D., Xiao, J.F., Zhu, D., Zhou, G.F., Guan, J.X., Liu, S.R., Zheng, W.Q., 2009. MELTS thermodynamic calculation of compositions of parental magma and fractional crystallization of the Jinchuan intrusion, Gansu Province. Acta Geological Sinica 83, 1302–1315 (in Chinese with English abstract).

Chen, L.-M., Song, X.-Y., Keays, R.R., Tian, Y.-L., Wang, Y.-S., Deng, Y.-F., Xiao, J.-F., 2013. Segregation and fractionation of magmatic Ni-Cu-PGE Sulfides in the Western Jinchuan intrusion, Northwestern China: insights from platinum group element geochemistry. Economic Geology 108, 1793–1811.

Chen, L.M., Song, X.Y., Danyushevsky, L.V., Wang, Y.S., Tian, Y.L., Xiao, J.F., 2015. A laser ablation ICP-MS study of platinum-group and chalcophile elements in base metal sulfide minerals of the Jinchuan Ni-Cu sulfide deposit, NW China. Ore Geology Reviews 65, 955–967.

Cocks, L.R.M., Torsvik, T.H., 2013. The dynamic evolution of the palaeozoic geography of eastern Asia. Earth Science Reviews 117, 40–79.

Cowgill, E., Yin, A.N., Harrison, T.M., Wang, X.-F., 2003. Reconstruction of the Altyn Tagh fault based on U-Pb geochronology: role of back thrusts, mantle sutures, and heterogeneous crustal strength in forming the Tibetan Plateau. Journal of Geophysical Research 108 (B7), 2346. http://dx.doi.org/10.1029/2002JB002080.

Dan, W., Li, X.-H., Guo, J., Liu, Y., Wang, X.-C., 2012. Paleoproterozoic evolution of the eastern Alxa block, westernmost North China: evidence from in situ zircon U-Pb dating and Hf-O isotopes. Gondwana Research 21, 838–864.

Davis, G.A., Qian, X.-G., Zheng, Y.-D., et al., 1996. Mesozoic deformation and plutonism in the Yunmeng Shan: a metamorphic core complex north of Beijing, China. In: Yin, A., Harrison, T.M. (Eds.), The Tectonic Evolution of Asia. Cambridge University Press, Cambridge, pp. 53–280.

Davis, G.A., Darby, B.J., Zheng, Y.-D., 2002. Geometric and temporal evolution of an extensional detachment fault, Hohhot metamorphic core complex, Inner Mongolia, China. Geology 30, 1003–1006.

de Jong, K., Xiao, W.J., Windley, B.F., Masago, H., Lo, C.H., 2006. Ordovician $^{40}Ar/^{39}Ar$ phengite ages from the blueschist-facies Ondor Sum subduction-accretion complex (Inner Mongolia) and implications for the early paleozoic history of

continental blocks in China and adjacent areas. American Journal of Science 306, 799–845.
de Waal, S.A., Xu, Zhanghua, Li, Chusi, Mouri, Hassina, 2004. Emplacement of viscous mushes in the Jinchuan ultramafic intrusion, western China. Canadian Mineralogist 42, 371–392.
Du, Y.-S., Zhu, J., Han, X., Gu, S.Z., 2004. From the back-arc basin to foreland basin-Ordovician-Devonian sedimentary basin and tectonic evolution in the North Qilian Orogenic belt. Geological Bulletin of China 23, 911–917 (in Chinese with English abstract).
Du, Y.-S., Zhu, J., Gu, S.Z., Xu, Y.J., Yang, J.H., 2007. Sedimentary geochemistry of the Cambrian-Ordovician cherts: implications on archipelago ocean of North Qilian Orogenic belt. Science in China Series D: Earth Sciences 50, 1628–1644.
Fan, H.R., Chen, F.K., Wang, K.Y., Xie, Y.H., Wilde, S., Satir, M., 2002. Zircon U-Pb age of a carbonatite dyke from Bayan Obo REE-Fe-Nb deposit, Inner Mongolia and its geological significance. Acta Petrologica Sinica 18, 363–368 (in Chinese with English abstract).
Gao, R., Cheng, X., Wu, G., 1999. Lithospheric structure and geodynamic model of the Golmud-Ejin transect in northern Tibet. In: Macfarlane, A., Sorkhabi, R.B., Quade, J. (Eds.), Himalaya and Tibet; Mountain Roots to Mountain Tops. Special Paper - Geological Society of America (GSA), Boulder, CO, United States, pp. 9–17.
Ge, X.H., Liu, J., 1999. Formation and tectonic background of the Northern Qilian Orogenic Belt. Earth Science Frontiers 6, 223–230 (in Chinese with English abstract).
Gehrels, G.E., Yin, A., Wang, X., 2003. Magmatic history of the northeastern Tibetan Plateau. Journal of Geophysical Research 108 (B9), 2423. http://dx.doi.org/10.1029/2002JB001876.
Geng, Y.S., Wan, Y.S., Shen, Q.H., Li, H.M., Zhang, R.X., 2000. Chronological framework of the Early Precambrian important events in the Lüliang area, Shanxi, Province. Acta Geologica Sinica 74, 216–223 (in Chinese with English abstract).
Geng, Y.S., Wang, X.S., Shen, Q.H., Wu, C.M., 2006. Redefinition of the Alxa Group complex (Precambrian metamorphic basement) in the Alxa area, Inner Mongolia. Geology in China 33, 138–145 (in Chinese with English abstract).
Gerya, T.V., Burg, J.-P., 2007. Intrusion of ultramafic magmatic bodies into the continental crust: numerical simulation. Physics of the Earth and Planetary Interiors 160, 124–142.
Grinenko, L.M., 1985. Sources of sulfur of the nickeliferous and barren gabbro-dolerite intrusions of the northwest Siberian platform. International Geology Review 28, 695–708.
Guo, Z.J., Zhang, Z.C., Jia, C., Wei, G., 2001. Tectonics of Precambrian basement of the Tarim craton. Science in China Series D: Earth Sciences 43, 229–236.
Holzheid, A., Grove, T.L., 2002. Sulfur saturation limits in silicate melts and their implications for core formation scenarios for terrestrial planets. American Mineralogist 87, 227–237.
Huang, H., Niu, Y., Nowell, G., Zhao, Z., Yu, X., Mo, X., 2014. The nature and history of the Qilian block in the context of the development of the Greater Tibetan Plateau. Gondwana Research 28, 209–224.
Jia, D.-C., Hu, R.-Z., Lu, Y., Qiu, X.-L., 2004. Collisional belt between the Khanka block and the North China block in the Yanbian region, Northeast China. Journal of Asian Earth Sciences 23, 211–219.
Kröner, A., Wilde, S., Wang, K., Zhao, G.C., 2002. Age and Evolution of a Late Archaean to Early Proterozoic Upper to Lower Crustal Section in the Wutaishan/Hengshan/Fuping Terrain of Northern China, a Field Guide. Geological Society of America Penrose Conference, Beijing, China.
Kröner, A., Wilde, S., Li, J., 2005. Age and evolution of a late Archean to early Paleoproterozoic upper to lower crustal section in the Wutaishan/Hengshan/Fuping terrain of northern China. Journal of Asian Earth Sciences 24, 577–595.
Kusky, T.M., Li, J.H., 2003. Paleoproterozoic tectonic evolution of the North China Craton. Journal of Asian Earth Sciences 22, 383–397.
Kusky, T.M., Santosh, M., 2009. The Columbia connection in North China. In: Reddy, S.M., Mazumder, R., Evans, D.A.D., Collins, A.S. (Eds.), Palaeoproterozoic Supercontinents and Global Evolution. Geological Society. Special Publications, London 323, pp. 49–71.
Kusky, T.M., Li, J.H., Santosh, M., 2007a. The Paleoproterozoic North Hebei orogen: North China craton's collisional suture with the Columbia supercontinent. In: Zhai, M.G., Xiao, W.J., Kusky, T.M., Santosh, M. (Eds.), Tectonic Evolution of China and Adjacent Crustal Fragments, Special Issue of Gondwana Research, 12, pp. 4–28.
Kusky, T.M., Windley, B.F., Zhai, M.G., 2007b. Tectonic evolution of the North China block: from orogen to craton to orogen. In: Zhai, M.G., Windley, B.F., Kusky, T., Meng, Q.R. (Eds.), Mesozoic Sub-continental Thinning Beneath Eastern North China, Geological Society. Special Publication, London 280, pp. 1–34.
Le Maitre, R.W., Streckeisen, A., Zanettin, B., Le Bas, M.J., Bonin, B., Bateman, P. (Eds.), 2002. Igneous Rocks: a Classification and Glossary of Terms: Recommendations of the International Union of Geological Sciences (IUGS) Subcommission on the Systematics of Igneous Rocks. Cambridge University Press, Cambridge, p. 252.
Lee, K.Y., 1985. Geology of the Tarim Basin with Special Emphasis on Petroleum Deposits, Xinjiang Uygur Zizhiqu, Northwest China. USGS Open-File Report 85-616, p. 56.
Lehmann, J., Arndt, N., Windley, B., Zhou, M.-F., Wang, C.Y., Harris, C., 2007. Field relationships and geochemical constraints on the emplacement of the Jinchuan intrusion and its Ni-Cu-PGE sulfide deposit, Gansu, China. Economic Geology 102, 75–94.
Li, W.Y., 1996. Metallogenic Series and Geochemistry of Nickel-copper Sulphide Deposits in China. Xi'an Cartongraphic Publishing House, Xi'an, p. 228 (in Chinese).
Li, C., Ripley, E.M., 2011. The giant Jinchuan Ni-Cu-(PGE) deposit: tectonic setting, magma evolution, ore genesis and exploration implications. Reviews in Economic Geology 17, 163–180.
Li, J.H., Kröner, A., Qian, X.-L., O'Brien, P., 2000. The tectonic evolution of early Precambrian high-pressure granulite belt, North China Craton (NCC). Acta Geological Sinica 274, 246–256.
Li, C., Xu, Z., de Waal, S.A., Ripley, E.M., Maier, W.D., 2004. Compositional variations of olivine from the Jinchuan Ni–Cu sulfide deposit, western China: implications for ore genesis. Mineralium Deposita 39, 159–172.
Li, X.-H., Su, L., Chung, S.-L., Li, Z.-X., Liu, Y., 2005. Formation of the Jinchuan ultramafic intrusion and the world's third largest Ni-Cu sulfide deposit: associated with the 825 Ma south China mantle plume? Geochemistry, Geophysics, Geosystems 6, 1–16.
Li, Z.-X., Bogdanova, S.V., Collins, A.S., Davidson, A., De Waele, B., Ernst, R.E., Fitzsimons, I.C.W., Fuck, R.A., Gladkochub, D.P., Jacobs, J., Karlstrom, K.E., Lu, S., Natapov, L.M., Pease, V., Pisarevsky, S.A., Thrane, K., Vernikovsky, V., 2008. Assembly, configuration, and breakup history of Rodinia: a synthesis. Precambrian Research 160, 179–210.
Lu, S.N., Wang, H.C., Li, H.K., 2002. Redefinition of the "Dakendaban Group" on the northern margin of the Qaidam Basin. Geological Bulletin of China 21, 19–23 (in Chinese with English abstract).
Lu, S.N., Li, H.K., Zhang, C.L., Niu, G.H., 2008. Geological and geochronological evidence for the Precambrian evolution of the Tarim Craton and surrounding continental fragments. Precambrian Research 160, 94–107.
Mavrogenes, J.A., O'Neill, H.St.C., 1999. The relative effects of pressure, temperature, and oxygen fugacity on the solubility of sulfide in mafic magmas. Geochimica et Cosmochimica Acta 83, 1173–1180.
Nakai, S., Masuda, A., Shimuzu, H., Qi, L., 1989. La-Ba dating and Nd and Sr isotope studies on the Baiyun Obo rare earth element ore deposits, Inner Mongolia, China. Economic Geology 84, 2296–2299.
Naldrett, A.J., 2004. The Jinchuan deposit, China. In: Naldrett, A.J. (Ed.), 2004, Magmatic Sulphide Deposits, Geology, Geochemistry and Exloration. Springer, pp. 373–404.
O'Brien, P.J., Rotzler, J., 2003. High-pressure granulites: formation, recovery of peak conditions and implications for tectonics. Journal of Metamorphic Geology 21, 3–20.
Peng, R., Zhai, Y., Li, C., Ripley, E.M., 2013. The Erbutu Ni-Cu deposit in the Central Asian Orogenic Belt: a Permian magmatic sulfide deposit related to boninitic magmatism in an arc setting. Economic Geology 108, 1879–1888.
Prichard, H., Knight, R., Fisher, P., McDonald, I., Zhou, M.-F., Wang, C., 2013. Distribution of platinum-group elements in magmatic and altered ores in the Jinchuan intrusion, China: an example of selenium remobilization by postmagmatic fluids. Mineralium Deposita 48, 767–786.
Ratschbacher, L., Franz, L., Enkelmann, E., Jonckheere, R., Pörschke, A., Hacker, B.R., Dong, S., Zhang, Y., 2006. The Sino-Korean-Yangtze suture, the Huwan detachment, and the Paleozoic-Tertiary exhumation of (ultra) high-pressure rocks along the Tongbai-Xinxian-Dabie Mountains. Geological Society of America Special Papers 403, 45–75.
RGST-QBMG (Regional Geological Survey Team of Qinghai Bureau of Mines and Geology), 1986. Eboliang Geologic Map (J-46-9), Scale 1:200,000, Qinghai Province Regional Geological Survey, Xining, China (in Chinese).
Ripley, E.M., Park, Y.R., Li, C., Naldrett, A.J., 1999. Sulfur and oxygen isotopic evidence of country rock contamination in the Voisey's Bay Ni-Cu-Co deposit, Labrador, Canada. Lithos 47, 53–68.
Ripley, E.M., Li, C., Shin, D., 2002. Paragneiss assimilation in the genesis of magmatic Ni-Cu-Co sulfide mineralization at Voisey's Bay, Labrador: $\delta^{34}S$, $\delta^{13}C$, and Se/S evidence. Economic Geology 97, 1307–1318.
Ripley, E.M., Lightfoot, P.D., Li, C., Elswick, E.R., 2003. Sulfur isotopic studies of continental flood basalts in the Noril'sk region: implications for the association between lavas and ore-bearing intrusions. Geochimica et Cosmochimica Acta 67, 2805–2817.
Ripley, E.M., Sarkar, A., Li, C., 2005. Mineralogic and stable isotope studies of hydrothermal alteration at the Jinchuan Ni-Cu deposit, China. Economic Geology 100, 1349–1361.
Ritts, B.D., Darby, B.J., Cope, T., 2001. Early Jurassic extensional basin formation in the Daqing Shan segment of the Yinshan belt, northern North China block, Inner Mongolia. Tectonophysics 339, 239–258.
S.G.U. (Sixth Geological Unit of Gansu Province, China), 1984. Geology of the Baijiaozuizi Cu-Ni Sulphide Deposit. Geological Publishing House, Beijing, People's Republic of China, p. 225 (in Chinese).
Song, X.-Y., Zhou, M.-F., Wang, C.Y., Qi, L., 2006. Role of crustal contamination in formation of the Jinchuan intrusion and its world-class Ni-Cu-(PGE) sulfide deposit, NW China. International Geology Review 48, 1113–1132.
Song, S.G., Zhang, L.F., Niu, Y.L., Wie, C.J., Liou, J.G., Shu, G.M., 2007. Eclogite and carpholite-bearing metasedimentary rocks in the North Qilian suture zone, NW China: implications for early palaeozoic cold oceanic subduction and water transport into mantle. Journal of Metamorphic Geology 25, 547–563.
Song, S.G., Niu, Y.L., Zhang, L.F., Wei, C.J., Liou, J.G., Su, L., 2009a. Tectonic evolution of early paleozoic HP metamorphic rocks in the North Qilian Mountains, NW China: new perspectives. Journal of Asian Earth Sciences 35, 334–353.
Song, X.-Y., Keays, R.R., Zhou, M.-F., Qi, L., Ihlenfeld, C., Xiao, J.-F., 2009b. Siderophile and chalcophile elemental constraints on the origin of the Jinchuan Ni-Cu-(PGE) sulfide deposit, NW China. Geochimica et Cosmochimica Acta 73, 404–424.

Song, X.-Y., Wang, Y.-S., Chen, L.-M., 2011. Magmatic Ni-Cu-(PGE) deposits in magma plumbing systems: features, formation and exploration. Geoscience Frontiers 3, 375–384.
Song, X.-Y., Chen, L.-M., Tian, Y.-L., Qiao, F.-G., 2012b. Simple Introduction of the Jinchuan Intrusion and Hosted Ni-Cu-(PGE) Ore Bodies. Post-Meeting Jinchuan Field Trip, 12th International Ni-Cu-(PGE) Symposium Guiyang, China, p. 9.
Song, S.-G., Su, L., Li, X.-H., Niu, Y.L., Zhang, L.F., 2012c. Grenville-age orogenesis in the Qaidam-Qilian block: the link between South China and Tarim. Precambrian Research 220–221, 9–22.
Song, X.-Y., Danyushevsky, L.V., Keays, R.R., Chen, L.-M., Wang, Y.-S., Tian, Y.-L., Xiao, J.-F., 2012a. Structural, lithological, and geochemical constraints on the dynamic magma plumbing system of the Jinchuan Ni-Cu sulfide deposit, NW China. Mineralium Deposita 47, 277–297.
Tang, Z.L., 1993. Genetic model of the Jinchuan nickel-copper deposit. In: Kirkham, R.V., Sinclair, W.D., Thorpe, R.I., Duke, J.M. (Eds.), Mineral Deposit Modelling, Geological Association of Canada, 40. Special Paper, pp. 389–401.
Tang, Z.L., Li, W.Y., 1995a. Mineralization Model and Geology of the Jinchuan Deposit Bearing PGE. Geological Publishing House, Beijing, p. 208 (in Chinese).
Tang, Z.L., Li, W.Y., 1995b. The Metallogenetic Model and Geological Contrast on the Jinchuan Platinum-bearing Ni-Cu Sulfide Deposit, 209. Geological Publishing House, Beijing (in Chinese with English abstract).
Tapponnier, P., Meyer, B., Avouac, J.P., Peltzer, G., Gaudemer, Y., Guo, S., Xiang, H., Yin, K., Chen, Z., Cai, S., Dai, H., 1990. Active thrusting and folding in the Qilian Shan, and decoupling between upper crust and mantle in northeastern Tibet. Earth and Planetary Science Letters 97, 382–403.
Tapponnier, P., Xu, Z., Roger, F., Meyer, B., Arnaud, N., Wittlinger, G., Yang, J., 2001. Oblique stepwise rise and growth of the Tibet Plateau. Science 294, 1671–1677.
Tung, K.A., Yang, H.Y., Liu, D.Y., Zhang, J.X., Tseng, C.Y., Wan, Y.S., 2007. SHRIMP U-Pb geochronology of the detrital zircons from the Longshoushan Group and its tectonic significance. Chinese Science Bulletin 52, 1414–1425.
Wan, Y.S., Xu, Z.Q., Yan, J.S., Zhang, J.X., 2001. Ages and compositions of the Precambrian high-grade basement of the Qilian Terrane and its adjacent areas. Acta Geologica Sinica 75, 375–384.
Wu, H.Q., Feng, Y.M., Song, S.G., 1993. Metamorphism and deformation of blueschist belts and their tectonic implications, North Qilian mountains, China. Journal of Metamorphic Geology 11, 523–536.
Xia, I.Q., Xia, Z.C., Xu, X.Y., Yang, H.Q., 1998. Proterozoic mid-ocean ridge, ocean island and back-arc basin volcanicm in the Qilian Mountains. Acta Geological Sinica 72, 301–312.
Xiao, W.-J., Windley, B.F., Hao, J., Zhai, M.-G., 2003. Accretion leading to collision and the Permian Solonker suture, Inner Mongolia, China: termination of the Central Asian orogenic Belt. Tectonics 22, 8.1–8.20.
Xiao, W.J., Windley, B.F., Yong, Y., Zhen, Y., Chao, Y., Liu, C.Z., Li, J., 2009. Early paleozoic to Devonian multiple-accretionary model for the Qilian Shan, NW China. Journal of Asian Earth Sciences 35, 323–333.
Xu, Y.G., Chung, S.L., Jahn, B.M., Wu, G.Y., 2001. Petrologic and geochemical constraints on the petrogenesis of Permian-Triassic Emeishan flood basalts in southwestern China. Lithos 58, 145–168.
Xu, X.-Y., Xia, L.-Q., Xia, Z.-C., 2005a. Volcanism and mineralization in the North Qilian Orogenic Belt, Northwestern China; mineral deposit research. In: Mao, J., Bierlein, F.P. (Eds.), Meeting the Global Challenge, Proceedings of the Eighth Biennial SGA Meeting Beijing, China, 18-21 August 2005, pp. 487–489.
Xu, B., Jian, P., Zheng, H., Zou, H., Zhang, L., Liu, D., 2005b. U-Pb zircon geochronology and geochemistry of Neoproterozoic volcanic rocks in the Tarim block of northwest China: implications for the breakup of Rodinia supercontinent and Neoproterozoic glaciations. Precambrian Research 136, 107–123.
Xu, B., Xiao, S., Zou, H., Chen, Y., Li, Z.-X., Song, B., Liu, D., Zhou, C., Yuan, X., 2009. SHRIMP zircon U-Pb age constraints on Neoproterozoic Quruqtagh diamictites in NW China. Precambrian Research 168, 247–258.
Yakubchuk, A., Degtyarev, K., Maslennikov, V., Wurst, A., Stekhin, A., Lobanov, K., 2012. Tectonomagmatic settings, architecture, and metallogeny of the Central Asian copper province. In: Hedenquist, J.W., Harris, M., Camus, F. (Eds.), Geology and Genesis of Major Copper Deposits and Districts of the World - a tribute to Richard H Sillitoe, Society of Economic Geologists, 16. Special Publication, pp. 403–432.
Yang, Z.D., Pan, X.S., Yang, Y.F., 1988. Tectonics and Minerals of Alashan Fault-block and Adjacent Area. Science Press, Beijing, pp. 46–80 (in Chinese with English abstract).
Yang, G., Du, A., Lu, J., Qu, W., Chen, J., 2005. Re-Os (ICP-MS) dating of the massive sulfide ores from the Jinchuan Ni-Cu-PGE deposit. Science in China Series D: Earth Sciences 48, 1672–1677.
Yin, A., Harrison, T.M., 2000. Geological evolution of the Himalayan-Tibetan orogen. Annual Reviews of Earth and Planetary Sciences 28, 211–280.
Yu, J.H., Wang, D.Z., Wang, C.Y., Wang, L.J., 2004. Paleoproterozoic granitic magmatism and metamorphism in middle part of Lüliang Range, Shanxi Province. Geological Journal of China Universities 10, 500–513 (in Chinese with English abstract).
Yue, Y.-J., Liou, J.-G., Graham, S.A., 2001. Tectonic correlation of Beishan and Inner Mongolia orogens and its implications for the palinspastic reconstruction of north China. In: Hendrix, M.S., Davis, G.A. (Eds.), Paleozoic and Mesozoic Tectonic Evolution of Central Asia: from Continental Assembly to Intracontinental Deformation, Geological Society of America, Memoirs, 194, pp. 101–116.
Zhai, M.-G., Santosh, M., 2011. The early Precambrian odyssey of the North China Craton: a synoptic overview. Gondwana Research 20, 6–25.
Zhai, M.G., Li, T.S., Peng, P., Hu, B., Liu, F., Zhang, Y.B., Guo, J.H., 2010. Precambrian key tectonic events and evolution of the North China Craton. In: Kusky, T.M., Zhai, M.G., Xiao, W.J. (Eds.), The Evolving Continents, 338. Geological Society of London Special Publications, pp. 235–262.
Zhang, Q., Wang, Y., Qian, Q., 2000. The North Qilian oceanic basin of the early Paleozoic age, a discussion with Ge, X.H. Geoscience 35, 121–128 (in Chinese with English abstract).
Zhang, C.L., Li, X.-H., Li, Z.-X., Lu, S.N., Ye, H.M., Li, H.M., 2007a. Neoproterozoic ultramafic-mafic-carbonatite complex and granitoids in Quruqtagh of northeastern Tarim block, western China: geochronology, geochemistry and tectonic implications. Precambrian Research 152, 149–169.
Zhang, J.X., Meng, F.C., Wan, Y.S., 2007b. A cold early Palaeozoic subduction zone in the North Qilian Mountains, NW China: petrological and U-Pb geochronological constraints. Journal of Metamorphic Geology 25, 285–304.
Zhang, M., Kamo, S., Li, C., Hu, P., Ripley, E., 2010. Precise U-Pb zircon-baddeleyite age of the Jinchuan sulfide ore-bearing ultramafic intrusion, western China. Mineralium Deposita 45, 3–9.
Zhang, J., Li, J., Liu, J., Feng, Q., 2011. Detrital zircon U-Pb ages of Middle Ordovician flysch sandstones in the western Ordos margin: new constraints on their provenances, and tectonic implications. Journal of Asian Earth Sciences 43, 1030–1047.
Zhao, T.P., Chen, F.K., Zhai, M.G., Xia, B., 2004. Single zircon U-Pb ages and their geological significance of the Damiao anorthosite complex, Hebei Province, China. Acta Petrologica Sinica 20, 685–690 (in Chinese with English abstract).
Zhao, G.C., Cawood, P.A., Li, S.Z., Wilde, S.A., Sun, M., Zhang, J., He, Y.H., Yin, C.Q., 2012. Amalgamation of the North China Craton: key issues and discussion. Precambrian Research 222–223, 55–76.
Zhou, M.F., Yang, Z.X., Song, X.Y., Lesher, C.M., Keays, R.R., 2002a. Magmatic Ni-Cu-(PGE) sulphide deposits in China. Canadian Institute of Mining, Metallurgy and Petroleum Special Volume 54, 619–636.
Zhou, T., Goldfarb, R.J., Phillips, G.N., 2002b. Tectonics and distribution of gold deposits in China - an overview. Mineralium Deposita 37, 249–282.
Zhu, L.D., Wang, C.S., Zheng, H.B., Xiang, F., Yi, H.S., Liu, D.Z., 2006. Tectonic and sedimentary evolution of basins in the northeast of Qinghai-Tibet Plateau and their implication for the northward growth of the Plateau. Palaeogeography, Palaeoclimatology, Palaeoecology 241, 49–60.